A glacial isostatic adjustment model for the central and northern Laurentide ice sheet based on relative sea level and GPS measurements

Simon, K. M.; James, T. S.; Henton, J. A.; Dyke, A. S.

DOI
10.1093/gji/ggw103

Publication date
2016

Document Version
Final published version

Published in
Geophysical Journal International

Citation (APA)
Simon, K. M., James, T. S., Henton, J. A., & Dyke, A. S. (2016). A glacial isostatic adjustment model for the central and northern Laurentide ice sheet based on relative sea level and GPS measurements. *Geophysical Journal International*, *205*(3), 1618-1636. Article ggw098. https://doi.org/10.1093/gji/ggw103

Geophysical Journal International

Geophys. J. Int. (2016) **205,** 1618–1636
Advance Access publication 2016 March 16
GJI Geodynamics and tectonics

doi: 10.1093/gji/ggw103

A glacial isostatic adjustment model for the central and northern Laurentide Ice Sheet based on relative sea level and GPS measurements

K.M. Simon,[1,2,3] T.S. James,[1,2] J.A. Henton[4] and A.S. Dyke[5,6]

[1]*School of Earth and Ocean Sciences, University of Victoria, Victoria, BC, Canada, V8P 5C2. E-mail: k.m.simon@tudelft.nl*
[2]*Geological Survey of Canada - Pacific, Natural Resources Canada, Sidney, BC, Canada, V8L 4B2*
[3]*Department of Geoscience and Remote Sensing, Delft University of Technology, Delft 2628 CN, The Netherlands*
[4]*Canadian Geodetic Survey, Natural Resources Canada, Sidney, BC, Canada, V8L 4B2*
[5]*Department of Earth Sciences, Dalhousie University, Halifax, Nova Scotia, Canada, B3H 4R2*
[6]*Department of Anthropology, McGill University, Montreal, Quebec, Canada, H3A 2T4*

Accepted 2016 March 10. Received 2016 March 8; in original form 2015 July 9

SUMMARY

The thickness and equivalent global sea level contribution of an improved model of the central and northern Laurentide Ice Sheet is constrained by 24 relative sea level histories and 18 present-day GPS-measured vertical land motion rates. The final model, termed Laur16, is derived from the ICE-5G model by holding the timing history constant and iteratively adjusting the thickness history, in four regions of northern Canada. In the final model, the last glacial maximum (LGM) thickness of the Laurentide Ice Sheet west of Hudson Bay was ∼3.4–3.6 km. Conversely, east of Hudson Bay, peak ice thicknesses reached ∼4 km. The ice model thicknesses inferred for these two regions represent, respectively, a ∼30 per cent decrease and an average ∼20–25 per cent increase to the load thickness relative to the ICE-5G reconstruction, which is generally consistent with other recent studies that have focussed on Laurentide Ice Sheet history. The final model also features peak ice thicknesses of 1.2–1.3 km in the Baffin Island region, a modest reduction relative to ICE-5G and unchanged thicknesses for a region in the central Canadian Arctic Archipelago west of Baffin Island. Vertical land motion predictions of the final model fit observed crustal uplift rates well, after an adjustment is made for the elastic crustal response to present-day ice mass changes of regional ice cover. The new Laur16 model provides more than a factor of two improvement of the fit to the RSL data (χ^2 measure of misfit) and a factor of nine improvement to the fit of the GPS data (mean squared error measure of fit), compared to the ICE-5G starting model. Laur16 also fits the regional RSL data better by a factor of two and gives a slightly better fit to GPS uplift rates than the recent ICE-6G model. The volume history of the Laur16 reconstruction corresponds to an up to 8 m reduction in global sea level equivalent compared to ICE-5G at LGM.

Key words: Satellite geodesy; Sea level change; Glaciology; Dynamics of lithosphere and mantle; North America.

1 INTRODUCTION AND PREVIOUS LAURENTIDE ICE SHEET STUDIES

During the last glaciation, large ice sheets covered much of North America, Greenland, Scandinavia and Antarctica, and at the Last Glacial Maximum (LGM, ∼24–14 ^{14}C kyr BP), almost all of northern Canada was covered by the Laurentide and Innuitian ice sheets (Dyke 2004). The large amount of water stored on land within the ice sheets caused globally averaged sea level to be between 120 and 130 m lower at LGM than at present (e.g. Fairbanks 1989; Yokoyama *et al*. 2000; Peltier & Fairbanks 2006; Austermann *et al*. 2013), but the weight of the ice depressed the Earth's crust and mantle so that in the vicinity of the ice sheets, relative sea level (RSL) was tens to hundreds of metres higher than at present (Walcott 1972). Following deglaciation, glacial isostatic adjustment (GIA) caused the land in regions near the former ice sheets to uplift, and relative sea level rapidly fell. In part owing to the great spatial lengths of shoreline indicating RSL history in the Canadian Arctic Archipelago, the history of postglacial sea level change in northern Canada is generally well recorded.

The spatial extent, flow history and chronology of the last North American glaciation has been constructed through

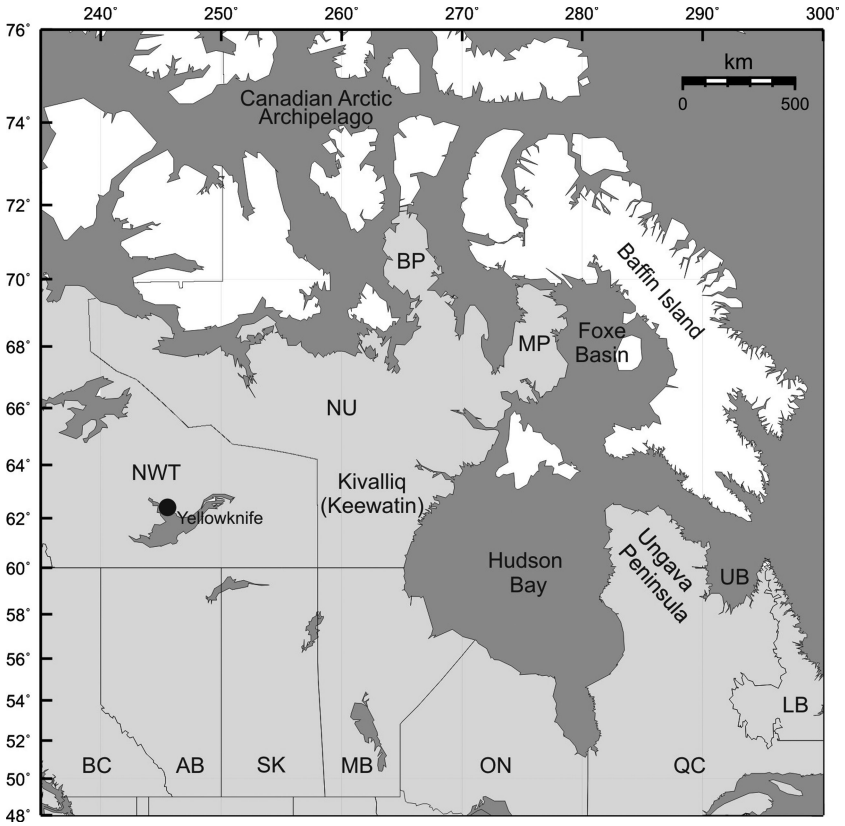

Figure 1. Regional map showing the study area and geographical place names mentioned in the text. Geographical place-name abbreviations are: BP, Boothia Peninsula; LB, Labrador; MP, Melville Peninsula; and UB, Ungava Bay. Canadian provincial and territorial abbreviations are: BC, British Columbia; AB, Alberta; SK, Saskatchewan; MB, Manitoba; ON, Ontario; QC, Quebec; NU, Nunavut; NWT, Northwest Territories. The islands of the Canadian Arctic Archipelago are shaded white.

glacial-geological observations of end moraines and other ice-marginal features, flow direction indicators, glacial erratic distributions and marine-limit and relative sea level measurements. These observations indicate that growth of the Laurentide Ice Sheet (LIS) from its last interstadial minimum commenced approximately 30–27 ^{14}C kyr BP (∼35–32 cal kyr BP) at the middle to late Wisconsinan transition (Dyke *et al*. 2002). The LIS reached its peak extent by approximately 24–21 ^{14}C kyr BP (∼29–25 cal kyr BP), and was confluent with the smaller Cordilleran Ice Sheet in western Canada and the Innuitian Ice Sheet to the north. Glacial flow indicators suggest that the thickest ice cover nucleated in three main regions over an area west of Hudson Bay, Quebec-Labrador and Foxe Basin (Fig. 1, Dyke *et al*. 1982, 2002). The LIS remained at near LGM conditions over North America until about 14 ^{14}C kyr BP (∼16.8 cal kyr BP). The main phase of deglaciation of the LIS occurred between 14 and 7 ^{14}C kyr BP (∼16.8–7.7 cal kyr BP), during which time there was a monotonic 90 per cent reduction in the area of the ice sheet complex relative to its area at LGM, including the ablation of marine-based ice in Hudson Bay between 8 and 7 ^{14}C kyr BP (∼8.8–7.7 cal kyr BP; Dyke 2004). By 5 ^{14}C kyr BP (∼5.9 cal kyr BP), deglaciation of North America was nearly complete, with the exception of remnant ice persisting on Baffin Island.

Many recent glacial isostatic adjustment studies in North America have considered the global ICE-5G ice sheet reconstruction of Peltier (2004), which was developed as an update to the ICE-4G reconstruction (Peltier 1994). ICE-5G was tuned to deliver a maximum eustatic sea level low-stand of ∼120–125 m, a value that is in accordance with the value determined from far-field sea level measurements by Fairbanks (1989) and Peltier & Fairbanks (2006). The model also generally well predicts sea level measurements and present-day vertical and horizontal motions over Fennoscandia (Peltier 2004; Argus & Peltier 2010). Based on the misfit between model predictions and present-day gravity and GPS data (Lambert *et al*. 2006; Argus & Peltier 2010; Mazzotti *et al*. 2011; Wang *et al*. 2013; Peltier *et al*. 2015), it has been shown that the ICE-5G reconstruction is too thick in the central sector of the Laurentide Ice Sheet (LIS) in the region west of Hudson Bay, throughout Manitoba and near Yellowknife. Misfits of ICE-5G to data in North America were similarly suggested by Braun *et al*. (2008) and van der Wal *et al*. (2008). Argus & Peltier (2010), additionally suggest that the ICE-5G model reconstruction is too thin near the British Columbia–Alberta border and in southern and eastern Quebec.

A successor model to ICE-5G, ICE-6G (Argus *et al*. 2014; Peltier *et al*. 2015) has been used in recent sea level and climate modelling studies (e.g. Engelhart *et al*. 2011; Toscano *et al*. 2011; Vettoretti & Peltier 2013). Relative to ICE-5G, Peltier *et al*. (2015) show that ICE-6G, with much thinner ice west of Hudson Bay, and moderately thicker ice in western Canada and northern Quebec, provides a better fit to GPS-measured vertical uplift rates in North America. Specifically, Vettoretti & Peltier (2013) describe ICE-6G, relative to ICE-5G, as being approximately 1500 m thinner in central Canada, as well as less than 1000 m thicker in both western Canada and northern Quebec. At ∼120 m, the eustatic sea level contribution of ICE-5G and ICE-6G are approximately equivalent (Vettoretti & Peltier 2013).

In this study, we revise ice thicknesses of the ICE-5G model in four regions of the northern and central Laurentide Ice Sheet to obtain improved fits with RSL and GPS data from northern Canada and to constrain sector-specific contributions to the global sea level budget. This study complements a previous study wherein a new model of the Innuitian Ice Sheet, which is located to the north of this study area, is developed (Simon *et al*. 2015). For this study, only the thickness history of ICE-5G is modified; the timing history is retained. The study region is northern Canada ($\geq$60°N) with particular focus placed on the Kivalliq (formerly Keewatin) region of Nunavut, northern Quebec and the Canadian Arctic Archipelago (Fig. 1). In contrast to the continental interior and the area that covers much of the southern extent of the last North American glaciation (focussed on by Argus & Peltier 2010) that has extensive GPS coverage and little to no RSL data, most of northern Canada has abundant RSL measurements and few permanent GPS sites. We therefore use late Pleistocene and Holocene RSL data as the primary constraint for the GIA models, and available present-day GPS observations as a secondary constraint. We compare the final model predictions to both ICE-5G and ICE-6G (detailed results of the latter comparison can be found in the supporting information). Relative to the starting model, the best-fitting model provides an improved fit to the RSL and the GPS data within the study region. The best-fitting model also provides updated estimates of the North American ice-volume history and its net contribution to global sea level that are smaller than those of both ICE-5G and ICE-6G.

2 DATA

2.1 Selection and analysis of the RSL data

The primary constraint for the GIA models in this study are relative sea level histories selected from a large database of measurements from the arctic and subarctic regions of Canada. The database is a compilation of radiocarbon ages from samples collected in North America by many different researchers over several decades. The database and the sea level measurements used in this study are provided in the supporting information. The sea level measurements consist of elevations and ages of radiocarbon-dated indicators of relative sea level position, such as marine shells, driftwood, mammal bones and plant material. The material type and stratigraphic context of the sea level indicators allows each sample to be classified according to whether sea level was located above, below, or near the elevation of each observation. This type of classification is also sometimes referred to as the 'indicative meaning' of an observation (Shennan 2007). The history of sea level change at a given location is then inferred by the line that most closely lies above the lower constraints and below the upper constraints. The position of sea level is most tightly constrained by measurements from interpreted near shore environments, or marine-terrestrial pairs of similar age and elevation.

The RSL database combines observations in a specified region to construct the history of sea level change. In some cases, especially in regions where data are sparse, measurements spaced up to approximately 150 km apart are combined to form a single sea level history. These larger sample regions, however, are used only in the central region where isostatic tilting is low. For sea level histories that encompass areas that have either large geographical extent or a complex deglaciation history (e.g. Churchill, Ungava Bay), groups of discrepant ages (i.e. where a few marine ages lie above terrestrial ages, or a few terrestrial ages lie below marine ages) within the same sea level history suggests that caution is needed when interpreting sea level change at these locations.

Within the study area, 24 relative sea level histories were chosen for comparison with the GIA model predictions (Fig. 2). The selected data sets favour sea level histories with observation points that: (1) lie geographically close together, (2) tightly constrain the position of sea level and (3) display continuity, both spatially and temporally, such that a well-defined sea level curve can be inferred. In addition, less well-defined sea level histories supplement the observations in geographical regions of interest, such as near load centres of the former ice sheet, or locations at or near continuous GPS sites. Because we calculate the fit of the model predictions relative to the individual measurements and not to the inferred sea level curve, it is not statistically meaningful to compare the GIA model predictions to measurements that lie far from the inferred position of sea level. We therefore exclude all non-constraining measurements when calculating the fit of the models to the data.

The criteria used to retain or exclude any given observation are as follows. Marine ages that clearly lie far below other marine constraints are excluded, provided that additional constraints exist within a $\pm$1 kyr time window of any excluded observation (Fig. 3). Terrestrial ages that clearly lie well above other terrestrial constraints are excluded in a similar manner. In portions of the relative sea level history where the position of sea level is unclear, or discrepant ages exist, all data points are retained in order to reflect the uncertainty of the observations (Fig. 3). Where groups of either marine ages or terrestrial ages are spaced closely together, all data points are retained. In addition, all nearshore sea level indicators, particularly shell ages of *Mytilus edulis*, a shallow-dwelling bivalve, are retained. Exclusion of the clearly non-constraining measurements minimizes scatter of the data set, and allows better quantitative comparison between the sea level data and the model predictions.

The difference between the relative sea level measurements and model predictions is determined by calculating the shortest distance in space and time (s, t) between each observation (o) to a point on the predicted sea level curve (p) (e.g. Mitrovica *et al*. 2000; Paulson *et al*. 2007). The fit of the predictions to the observations at each site location is then evaluated by a χ^2 measure of misfit using

$$\chi^2_{\mathrm{RSL}} = \frac{1}{N}\sum_{i=1}^{N}\left[\left(\frac{s_i^o - s_i^p}{\sigma_i^s}\right)^2 + \left(\frac{t_i^o - t_i^p}{\sigma_i^t}\right)^2\right], \quad (1)$$

where (s_i^o, t_i^o) is the elevation and age of an RSL measurement, and (s_i^p, t_i^p) is the elevation and age of the nearest point on the predicted curve, ${\sigma_i}^s$ and ${\sigma_i}^t$ are the respective uncertainties in space and time of the ith observation, and N is the number of observations.

The age error of each observation is derived from the radiocarbon-laboratory estimate. The elevation errors of the observations reflect both the elevation measurement error and the uncertainty associated with the interpretation of the vertical position of each sample relative to past sea level. Similar to Peltier (1998), we calculate the vertical error as a function of sample elevation. For observations below 5 m, the vertical error is calculated as 20 per cent of the measured elevation, with a minimum error of 0.5 m. Between 5 and 20 m elevation, observations are assigned a vertical error of $\pm$1 m. Above 20 m elevation, the vertical error is calculated as 5 per cent of the observed elevation. In addition, we include an uncertainty of $\pm$5 m on each marine age to represent uncertainty in growth depth or tidal range. Including this additional uncertainty reduces the calculated χ^2 values, but does not affect inferences of optimal parameter values.

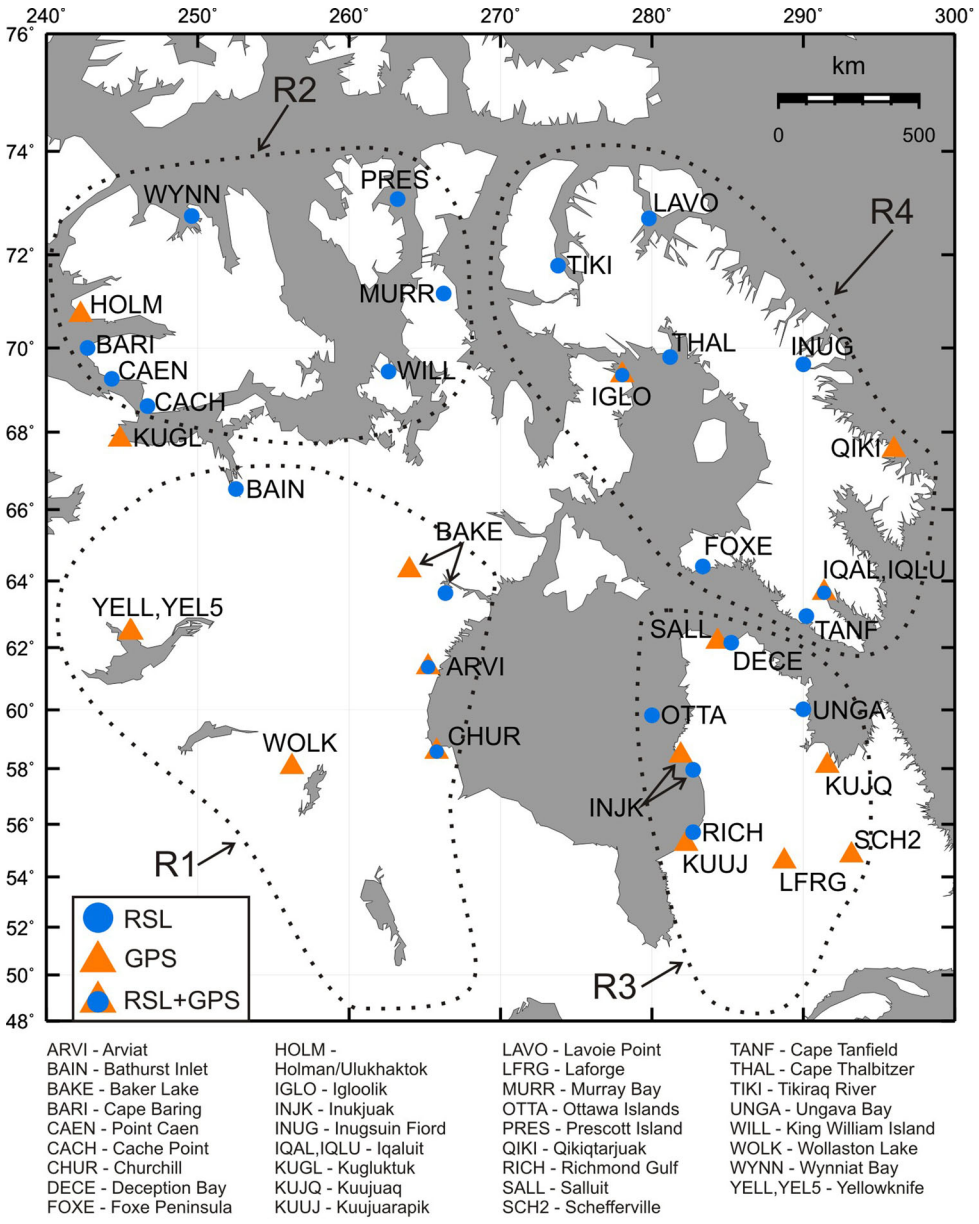

Figure 2. Site map showing the relative sea level (RSL) and GPS site locations and names. The RSL data are described in more detail in the supporting information; the GPS data are given in Table 1. Approximate boundaries of the four regions (R1–R4) of study are indicated by the black dotted lines.

In the χ^2 calculation, the relative sea level observations are categorized as either upper or lower constraints on the position of sea level and there is no additional category for nearshore constraints. Therefore, nearshore sea level indicators are not more heavily weighted in the χ^2 calculation than the other constraints. Independent consideration of nearshore sea level indicators would, however, have the advantage that predicted sea level is preferentially fit to the data points that provide the tightest constraint on the position of sea level. A limitation associated with not having a separate nearshore indicator in the χ^2 calculations is that in cases where the data are comprised predominantly of one type of constraint, the best-fitting prediction may be biased. This bias may occur, for example, for predictions of sea level that are above a set of predominately marine indicators; in principle, any sea level prediction above a marine constraint is considered equally valid, but the χ^2 calculations will worsen as the overprediction increases and the inferred best-fitting value may therefore be biased too low (the same is true for underpredicted values of sea level relative to terrestrial constraints). However, our selection of relative sea level histories that have either a good distribution of both upper and lower constraints, or are dominated by nearshore indicators, substantially mitigates this effect for most site locations in this study. In these cases, the method of data filtering described above yields a robust measure of model misfit to the data.

The radiocarbon ages of the relative sea level measurements are normalized for isotopic fractionation relative to $\delta^{13}C = -25‰$ following the conventions of Stuiver & Polach (1977). Throughout the study area, radiocarbon ages from marine shells and mammals are corrected for the reservoir effect using regional corrections (McNeely *et al*. 2006). Marine algae ages from samples collected west of Hudson Bay are corrected using the regional reservoir correction determined by Simon *et al*. (2014). The radiocarbon ages (and age errors) of the samples are calibrated to calendar years using the program Calib 5.1 (Stuiver & Reimer 1993). Marine ages are

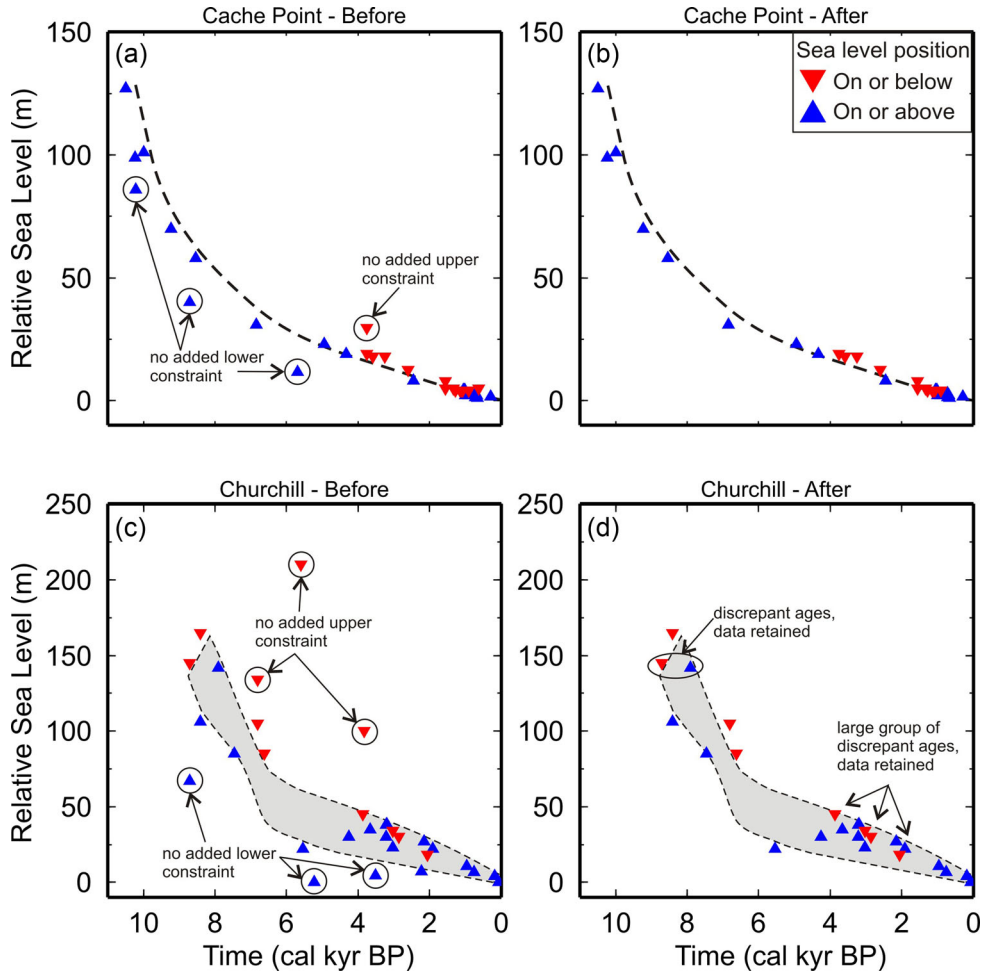

Figure 3. Examples of the criteria used for excluding or retaining data points from the relative sea level histories. Marine ages occur below sea level and are shown by the blue triangles. Terrestrial ages occur above sea level and are shown by the red triangles (the triangles point in the direction of inferred sea level). Marine (terrestrial) ages that lie well below (above) the inferred position of sea level are excluded; ambiguous or discrepant ages are retained. The top panels show the relative sea level history of a clearly constrained site location (Cache Point) before and after the filtering criteria are applied. At Cache Point, the inferred position of sea level is shown by the black dashed line. The bottom panels show the relative sea level history of a less clearly constrained location (Churchill) before and after the filtering criteria are applied. At Churchill, the inferred position of sea level is enclosed within the grey-shaded envelope. The larger scatter on the Churchill data set results in overall larger calculated misfit values.

calibrated using the Marine04 data set (Hughen *et al*. 2004), and terrestrial ages are calibrated using the IntCal04 data set (Reimer *et al*. 2004). In the supporting information, the relative sea level histories for each of the 24 locations are given in two formats: (i) the data before age calibration and removal of non-constraining points and (ii) the data after these changes.

2.2 GPS data and elastic correction

Within the study area, the measured vertical land motion rates of 18 GPS sites are considered (Fig. 2, Table 1). Rates of horizontal motion are available in Table S2. All GPS data, except for Arviat, are processed using the Bernese GPS Software Version 5.0 (Dach *et al*. 2007). Weekly solutions from continuous sites are combined into a single cumulative (multiple-epoch) solution to provide estimates of both station coordinates and their velocities with respect to a consistent global reference frame (Craymer *et al*. 2011). In order to provide an increased spatial sampling of crustal deformation in Canada, we also estimate velocities at sites of the Canadian Base Network (CBN) by combining repeated multiple-epoch (episodic) GPS measurements. Initiated in 1994, the CBN is a Canada-wide network of high-stability pillar monuments with forced-centring mounts for GPS receiver antennas. CBN solutions for each measurement epoch are also systematically combined into a single Canada-wide, multi-epoch cumulative solution. Using the Canadian Geodetic Survey's SINEX combination software, the continuous and episodic networks are integrated and aligned to the ITRF2008 reference frame (Altamimi *et al*. 2011). Arviat is a campaign GPS site whose processing is outlined in Simon *et al*. (2014). The misfit between the observed and predicted present-day rates of vertical land motion is calculated using a mean squared error (MSE) measure of misfit

$$\mathrm{MSE}_{\mathrm{GPS}} = \frac{1}{N}\sum_{i=1}^{N}\left(V_i^o - V_i^p\right)^2, \qquad (2)$$

where V_i^o and V_i^p are the observed and predicted rates of vertical crustal motion at the ith site location, respectively, and N is the number of GPS sites.

In the Canadian Arctic Archipelago, glaciers and ice caps (GIC) are present on Baffin, Devon, Axel Heiberg and Ellesmere islands. These glaciers and ice caps, as well as the nearby Greenland Ice Sheet, are experiencing rapid present-day mass loss (e.g. Gardner

Table 1. Vertical crustal motion rates derived from GPS observations and predicted from present-day ice change, as described in Section 2.2.

GPS site[a]	Latitude (°N)	Longitude (°E)	Vertical crustal motion (mm yr^{-1})	Vertical uncertainty (mm yr^{-1})	Vertical elastic response (mm yr^{-1})[b]	Time span (yr)	Number of epochs or per cent usable data[c]
Regions 1 and 2							
ARVI	61.08	265.93	9.250	1.250	0.56	2009.5164–2012.8101	3
BAKE*	64.32	264.00	11.181	0.131	0.64	2002.1233–2011.2822	71 per cent
CHUR*	58.76	265.91	10.873	0.081	0.57	2000.0137–2011.2822	93 per cent
HOLM*	70.74	242.24	2.547	0.116	0.72	2001.6603–2011.2822	99 per cent
KUGL	67.82	244.87	5.757	1.544	0.65	2000.6406–2011.4873	4
WOLK	58.06	256.20	8.114	0.769	0.51	1995.7364–2011.4873	5
YELL*	62.48	245.52	6.309	0.055	0.58	2000.0137–2011.2822	95 per cent
YEL5	62.47	245.62	7.063	0.820	0.58	1996.5503–2011.4873	5
Region 3							
INJK	58.46	281.89	11.468	1.346	0.61	1997.5338–2010.4982	4
KUJQ	58.11	291.59	9.089	1.317	0.67	1997.5338–2010.4982	4
KUUJ*	55.28	282.25	14.364	0.321	0.53	2002.5425–2011.2822	90 per cent
LFRG	54.60	288.73	13.584	0.847	0.56	1997.5338–2011.7501	7
SALL	62.19	284.33	7.729	1.405	0.85	1997.5338–2010.4982	4
SCH2*	54.83	293.17	11.396	0.063	0.60	2000.0137–2011.2247	97 per cent
Region 4							
IGLO	69.38	278.19	10.570	1.790	1.51	2000.6406–2010.4982	3
IQAL*	63.76	291.49	4.811	2.840	1.10	2009.7480–2011.2822	100 per cent
IQLU	63.75	291.45	3.128	1.438	1.10	2000.6406–2010.4982	5
QIKI*	67.56	295.97	3.388	0.115	2.94	2004.5547–2011.2822	100 per cent

[a]Continuous GPS sites are marked with an asterisk (*).
[b]The prediction for elastic vertical motion due to present-day ice mass loss that is applied to the model-predicted vertical rates is also given.
[c]The number of epochs or percentage of usable data is indicated for episodic and continuous sites, respectively.

et al. 2011; Rignot *et al*. 2011; Shepherd *et al*. 2012; Bolch *et al*. 2013; Gardner *et al*. 2013). In addition to uplift from the long-term GIA response, observed rates of vertical land motion in parts of our study area may contain a significant component of uplift attributable to the elastic response of the Earth to changes in present-day regional ice cover. Using an elastic earth model and ice cover that approximates present-day changes to the northern GIC, and the Greenland Ice Sheet, we compute a correction for this effect (Table 1), following the description of Simon *et al*. (2015). Based on recent estimates, we specify rates of present-day mass loss of -60 and -142 Gt yr^{-1} for the Canadian Arctic GIC and Greenland, respectively (Shepherd *et al*. 2012; Gardner *et al*. 2013). Uniform mass loss is assumed for both regions. In parts of our study area that are close to regions experiencing present-day ice mass loss (such as Baffin Island and to a lesser extent Ungava Peninsula) estimating the magnitude of the mass loss effect will allow us to evaluate the relative importance of incorporating this effect into predicted vertical uplift rates.

3 METHODS

3.1 Model description

The GIA model consists of a global ice sheet reconstruction that varies in space and time, and an earth model that describes the Earth's response to surface loading. The starting ice sheet model is the global ICE-5G v1.2 reconstruction (Peltier 2004), which uses the ice sheet margin chronology of Dyke *et al*. (2003), and whose timing spans the last glacial period (122 kyr–present). The ice sheet history is applied to a spherically symmetric earth model with a compressible elastic lithosphere overlying a compressible linear viscoelastic mantle. Our reference earth model follows the VM5a profile of Peltier & Drummond (2008) and consists of a 60-km-thick elastic lithosphere overlying a 40-km-thick high-viscosity (10^{22} Pa s) layer. At greater depths, the VM5a viscosity profile is similar to the VM2 profile derived from the global mantle viscosity estimate of Peltier (1996). VM5a has viscosities of 5×10^{20} Pa s from 100 to 660 km depth, 1.6×10^{21} Pa s between 660 and 1160 km depth and 3.2×10^{21} Pa s from 1160 km depth to the core mantle boundary. The Earth's density and rigidity parameters are averaged values from the Preliminary Reference Earth Model (Dziewonski & Anderson 1981).

The model calculations include a global, gravitationally self-consistent solution of the sea level equation following the methods described by Mitrovica & Peltier (1991), expanded by Mitrovica & Milne (2003) and Kendall *et al*. (2005) and as implemented by Simon (2014). The effects of time-varying ocean–continent geometry and water dumping into regions of formerly grounded marine-based ice are modelled following the methodology of Mitrovica & Milne (2003). The model predictions are generated in the centre of mass reference frame, and the computational algorithm follows the pseudospectral approach of Mitrovica *et al*. (1994), with all calculations truncated at spherical harmonic degree and order 128. The grid cell spacing in the ice sheet model is approximately $0.7^\circ \times 0.7^\circ$. The spacing of the grid is uniform, and does not vary between central regions of the ice sheet (where ice surface slopes are minimal) and more marginal regions (where ice surface slopes are large).

3.2 Modelling approach

The revisions to the GIA model explore variations to the thickness of the starting ice sheet reconstruction. Two constraints on the model

are prescribed at the outset of the study and held fixed during the model revisions: the timing history of the ice sheet model, and the earth model. We have focussed on the thickness history of the ice sheet model and found that improvements to the fit of model predictions to RSL and GPS data could be obtained without introducing revisions to the timing of the ice sheet history or revisions to the earth model.

Based on a combination of geographical and glaciological boundaries, the study area is divided into four smaller regions (Fig. 2). The first region is the Kivalliq (formerly Keewatin) region west of Hudson Bay, which is one of the former load centres of the Laurentide Ice Sheet. This region also includes parts of Hudson Bay, the Northwest Territories, Saskatchewan and Manitoba. Region 2 lies to the north of Region 1, and includes Boothia Peninsula and the southernmost islands of the Canadian Arctic Archipelago, excluding Baffin Island. Both Region 1 and Region 2 are within the Keewatin Sector of the LIS, but Region 2 is in a zone peripheral to the main load centre, and is therefore treated separately from Region 1. Region 3 is east of Hudson Bay, and includes Ungava Peninsula in northern Quebec. Region 4 consists of Baffin Island, Foxe Basin and Melville Peninsula, roughly equivalent to the Baffin Sector of the LIS. The southern portions of Region 1 (mainly Manitoba) and Region 3 (southern Quebec) have little RSL data, and thus are not areas of primary focus of our study. However, in order to maintain regional continuity in the history of ice sheet thickness (and surface elevation), changes to the ice sheet model extend to include the southern portions of both regions. Modification of the load in these regions also is consistent with Argus & Peltier (2010), who identify both Manitoba and southern Quebec as regions characterized by significant misfits between ICE-5G model predictions and observations.

Each of the regions is considered sequentially, and the best-fitting model of the preceding region is carried forward to the next region. The sequential approach introduces a degree of non-uniqueness to the modifications since changes made to the ice sheet in one region may influence model predictions in neighbouring regions. However, we find that the sequential (region by region) predictions differ little from the corresponding predictions of the final model, suggesting that if load revisions had been carried out over the entire study area simultaneously a final model would have resulted that is similar to the sequential final model presented here. The location of each predicted relative sea level curve is the average latitude and longitude of all of the data points that comprise that site's sea level history, while present-day rates of vertical motion are computed at the precise locations of the GPS sites. RSL and GPS site locations that are close together may share the same site name (e.g. BAKE, INJK and IGLO, Fig. 2). Ice sheet thickness scaling factors are generally applied to groups of grid cells within each region. Where finer spatial detail appears warranted, individual grid cells are modified. The scaling factors for the best-fitting model are provided in the supporting information.

4 VARIATIONS TO ICE SHEET HISTORY

4.1 Regions 1 and 2

Of the regions considered in this study, Region 1 has the fewest available RSL measurements. The four main relative sea level histories that exist in the region are located at Arviat, Baker Lake, the southern end of Bathurst Inlet and Churchill (ARVI, BAKE, BAIN and CHUR). At Arviat, Simon *et al*. (2014) recently improved the RSL history, and presented a campaign GPS uplift rate for site ARVI. Baker Lake and Churchill have permanent GPS sites (BAKE and CHUR), and within the continental interior of Region 1, there are also GPS sites at Wollaston Lake (WOLK) and Yellowknife (YELL and YEL5). The original ICE-5G model strongly overpredicts both Holocene RSL change and present-day vertical motion rates in Region 1 (Figs 4 and 5).

Because Region 1 is very large and because both the RSL and GPS data sets are consistently overpredicted by the original model, we begin by performing a sensitivity analysis wherein the thickness of the central LIS is uniformly scaled to identify a general best-fitting scaling factor for this region (similar to Simon *et al*. 2014). We then consider more localized adjustments to the load in Region 1. The applied scaling factors range from 0.4–1.2. At Arviat and Bathurst Inlet, the RSL misfit is minimized for scaling factors of 0.6–0.7 (Fig. 6). At Baker Lake, which is located in a region slightly peripheral to the load centre, scaling factors of 0.7–0.8 provide the best fit to the RSL data. Finally, at Churchill, the misfit appears minimized for larger reductions to the load thickness, or scaling factors of 0.4–0.6. The large scatter on the Churchill data yields overall higher χ^2 values relative to the other sites, and the existence of discrepant ages within the Churchill data set suggests that the relative sea level measurements require either more detailed filtering of the data or spatial separation of the measurements into two or more sea level histories. At Churchill, models with higher scaling factors of 0.6–0.7 appear to fit well the late Holocene sea level data despite the poor fit with the early Holocene data (Fig. 4).

In Region 1, the GPS-measured vertical land motion rates also indicate that a reduced load thickness relative to ICE-5G is needed (Fig. 5). The original model overpredicts present-day uplift rates at all five sites, including Yellowknife, Baker Lake and Churchill, which were also shown to be overpredicted by Argus & Peltier (2010). The MSE misfit value of the present-day vertical rates is reduced from 15.2 $mm^2\ yr^{-2}$ for the original model (1.0 scaling factor), to 2.0 $mm^2\ yr^{-2}$ for the 0.7 scaling factor model. For the 0.7 scaling factor model, the fit of the present-day uplift rate is improved at Yellowknife, Wollaston Lake, Arviat and Churchill. At Baker Lake, the fit of the predicted uplift rate is worsened for the 0.7 scaling factor model relative to the original model, and the predicted rate also switches from being too large to being too small. This result suggests that either the 30 per cent reduction is too large at Baker Lake, or alternatively, that Baker Lake deglaciated later than modelled in ICE-5G. We therefore apply smaller scaling factors of 0.9 to the ice sheet thickness north of Baker Lake while maintaining the 0.7 scaling factor elsewhere. This localized modification yields an improved fit to the RSL data at Baker Lake, and increases the predicted present-day uplift rate from 8.6 to 10.0 mm yr^{-1} (Fig. 5). The localized change to the load near Baker Lake does not significantly change the predicted RSL fall or rates of vertical uplift at other sites in Region 1. Improving the fit at Baker Lake further reduces the regional MSE misfit on the GPS observations from 2.0 to 1.3 $mm^2\ yr^{-2}$.

The ice load around Churchill is not locally decreased based on the RSL χ^2 values, because discrepant ages in the RSL data make the sea level history harder to interpret, and because the late Holocene sea level history is well fit by a 0.7 scaling factor. Also, although the predicted present-day uplift rate is improved for the 0.7 scaling factor model relative to the original model at Churchill, the predicted rate changes from being too large to too small, and further reductions to the ice sheet thickness would only worsen this trend. The best-fitting model for Region 1 therefore has a scaling factor of 0.7 applied throughout most of the region, and a smaller scaling factor of 0.9 applied locally north of Baker Lake.

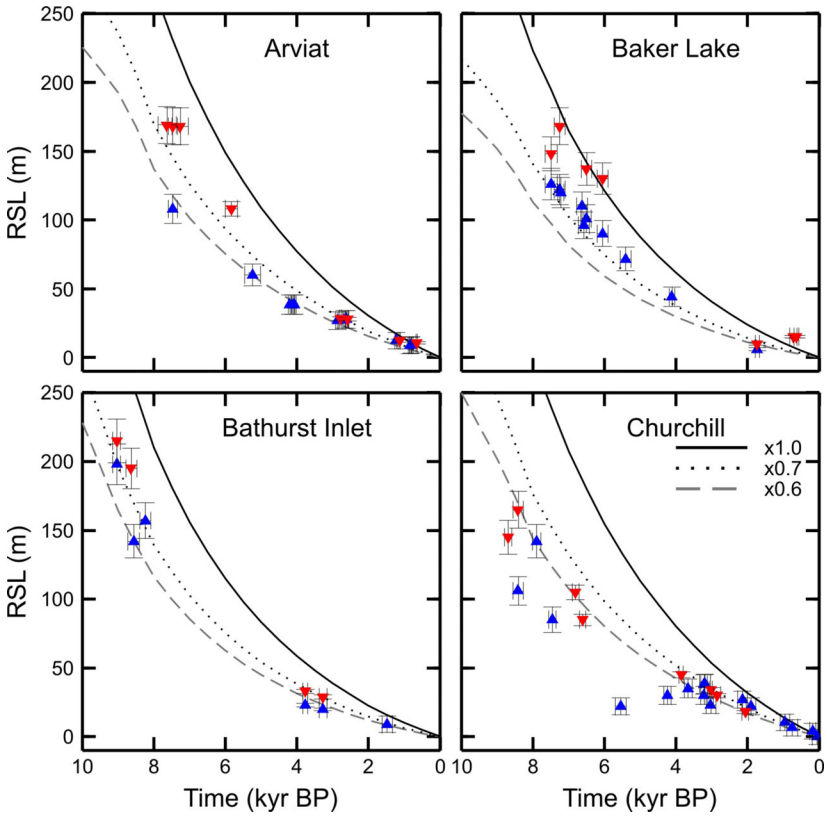

Figure 4. Relative sea level predictions and measurements for Region 1. Lower observational constraints are shown by blue triangles; sea level was at or above these points. Upper observational constraints are shown by red triangles; sea level was at or below these points. Triangles point in the direction of the inferred position of sea level. The starting ice sheet reconstruction (black line, ×1.0) overpredicts sea level at all four locations in Region 1. Model predictions where the regional ice load has been scaled by factors of 0.7 (black dotted line) and 0.6 (grey dashed line) provide a better fit to the observations.

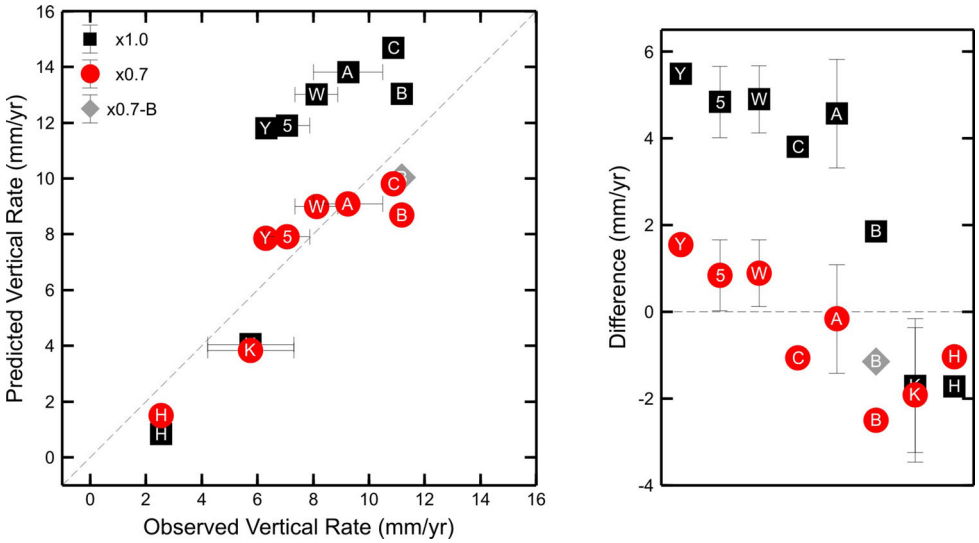

Figure 5. Predicted versus GPS-observed vertical rates of uplift in Regions 1 and 2 (left-hand panel), and the differences between the predicted and observed rates (right-hand panel). The starting model (black squares, ×1.0) overpredicts rates of vertical uplift at all locations in Region 1, and underpredicts these values for both locations in Region 2. An ice sheet reconstruction reduced by 30 per cent in Region 1 improves the fit of the predictions to the data (red circles). Additional local adjustments to the ice load around Baker Lake further improve the fit at that location (grey diamond). All predictions include the component of uplift resulting from present-day mass loss of Arctic glaciers and ice caps, and the Greenland Ice Sheet, as discussed in the text. A, Arviat; B, Baker Lake; C, Churchill; H, Holman; K, Kugluktuk; W, Wollaston Lake; Y, Yellowknife (site YELL); 5-Yellowknife (site YEL5).

Region 2 lies directly to the north of Region 1, within the Keewatin Sector of the LIS but farther from the load centre. The seven relative sea level histories considered in this region are Cache Point, Point Caen, Cape Baring, Wynniatt Bay, King William Island, Murray Bay and Prescott Island (CACH, CAEN, BARI, WYNN, WILL, MURR and PRES, respectively, Fig. 2). In or near Region 2, GPS observations exist at Kugluktuk (KUGL) and Ulukhaktok (formerly Holman, HOLM). We make no changes to the ice sheet

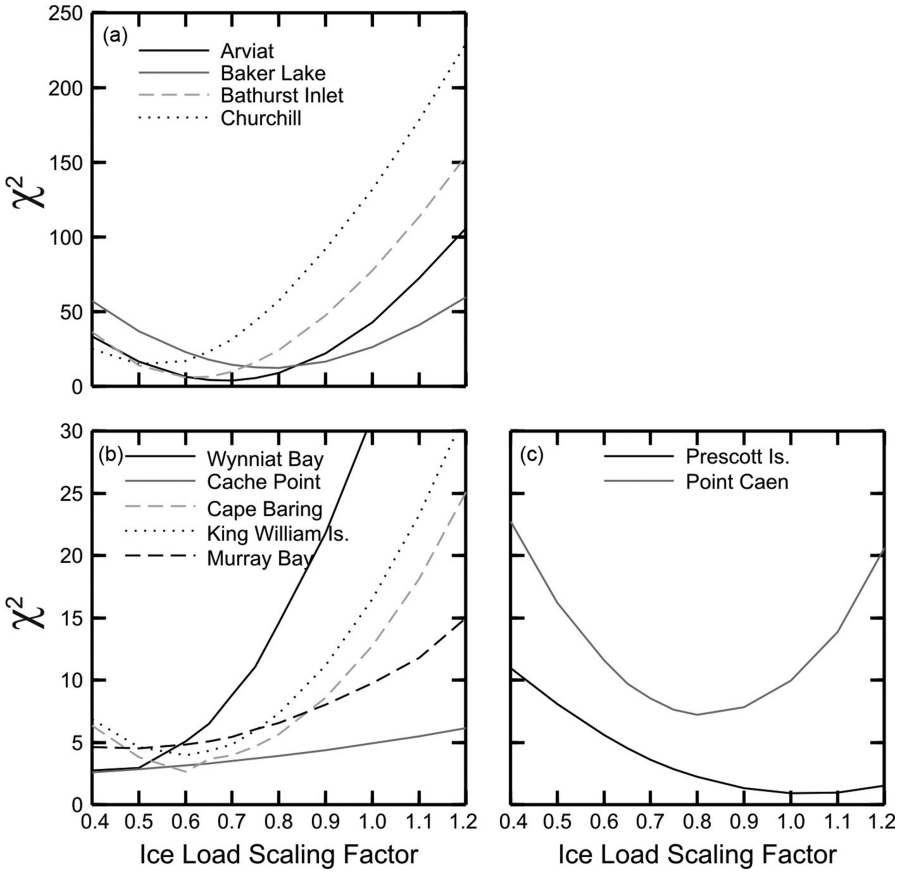

Figure 6. Calculated χ^2 misfits of the relative sea level predictions, compared to the relative sea level measurements, for (a) Region 1 and (b and c) Region 2. For all panels, the sensitivity analysis scales the starting ICE-5G load reconstruction (equivalent to a 1.0 scaling factor) in Region 1 by scaling factors that range from 0.4 to 1.2, while the thickness history of Region 2 remains unchanged. (a) In Region 1, the misfit of RSL predictions to observations is minimized for an approximately ∼30 per cent reduction to the starting load thicknesses within that region. (b, c) In Region 2, the fit of RSL predictions to RSL data also generally is improved for reduced versions of the ice sheet reconstruction in Region 1. The χ^2 misfits of most sites in Region 2 are minimized for Region 1 scaling factors of 0.5–0.7 (b), although at Point Caen and Prescott Island, the misfit is minimized for larger scaling factors (c). Note (a) uses a different vertical scale than (b) and (c).

thicknesses in Region 2. Instead, we note the effect of load reductions in Region 1 on relative sea level predictions in Region 2, and we find that an improved fit is obtained.

While reducing the ice sheet thickness in Region 1 reduces the amplitude of predicted sea level in that region, the reduced Region 1 load thickness increases the amplitude of predicted sea level in Region 2 (Fig. 7). This result is because the component of lithospheric depression due to the Region 2 ice load remains unchanged, while the component of lithospheric uplift in Region 2 that is induced by the large load centre to the south in Region 1 is reduced. The net result is that the lithospheric depression in Region 2 is increased, and the predicted position of sea level change increases. The original model tends to underpredict sea level in Region 2, and overall the fit of the model predictions to the RSL data is improved for Region 1 scaling factors of less than 1 (Fig. 6).

At Cape Baring, Wynniatt Bay, King William Island and Murray Bay, the misfit of the relative sea level predictions to the observations is minimized for Region 1 scaling factors of 0.6–0.7 (Fig. 6). The fit is also marginally improved at Cache Point and Point Caen for scaling factors less than 1. The fit at Prescott Island is not improved for the reduced scaling factors, although the χ^2 value at this location for a scaling factor of 0.7 is still comparable to the minimized χ^2 values of the other sites. The total misfit value for all seven RSL sites for the 1.0 scaling model is χ^2_{tot} (1.0) = 10.4, while for the 0.7 scaling factor model χ^2_{tot} (0.7) = 6.1. Thus, reducing the load thicknesses in Region 1, and making no changes to the load history in Region 2, decreases the misfit to the RSL data in Region 2 by approximately 40 per cent. At GPS sites KUGL and HOLM, the reduced load thickness model yields predicted vertical motion rates that are unchanged, and slightly improved, respectively (Fig. 5).

4.2 Region 3

Region 3 lies east of Hudson Bay, and encompasses much of Quebec. This region has only moderately well constrained relative sea level histories. The sea level histories considered in this region are from the Ottawa Islands, Inukjuak, Deception Bay, the western shoreline of Ungava Bay and Richmond Gulf (OTTA, INJK, DECE, UNGA, RICH, respectively). The sea level record at Richmond Gulf is very well constrained; unlike any of the other sea level histories shown in this study, the marine ages shown in the sea level curve for Richmond Gulf were obtained only from shells of the shallow-water *Mytilus edulis* species, and therefore place a tight constraint on the position of sea level. On Ungava Peninsula, there are GPS sites at Inukjuak, Salluit and Kuujuaq (INJK, SALL and KUJQ). East of Hudson Bay and south of Ungava Peninsula, we also consider the GPS-measured vertical motion rates at Kuujjuarapik, Laforge and Schefferville (KUUJ, LFRG and SCH2).

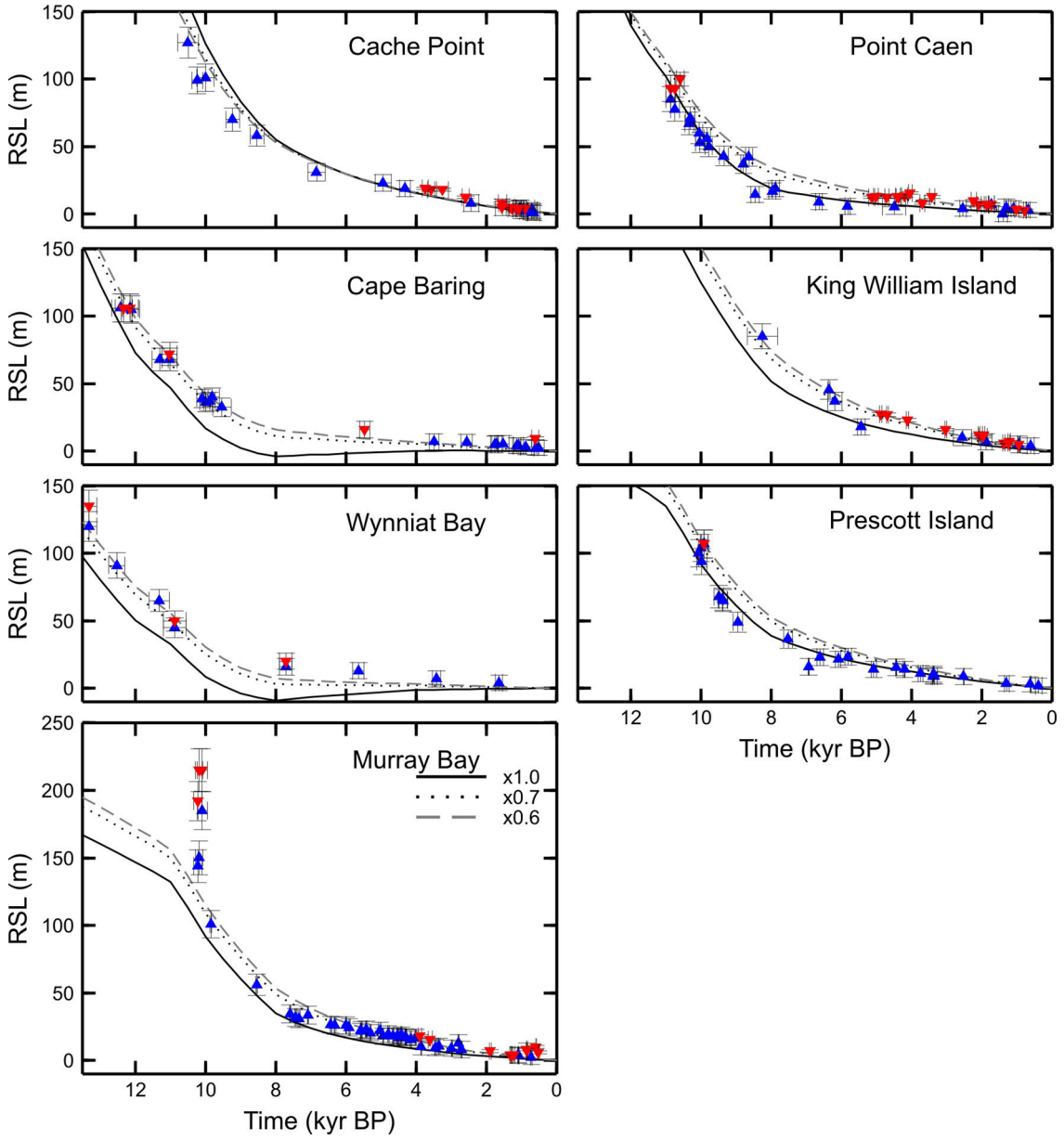

Figure 7. Relative sea level predictions and measurements for Region 2. Sea level measurements are plotted as described in the caption to Fig. 4. The starting ice sheet reconstruction (black line, ×1.0) underpredicts sea level at several locations in Region 2. Model predictions where the ice load in Region 1 has been scaled by factors of 0.7 (black dotted line) and 0.6 (grey dashed line) provide a better fit to the observations. The ice load in Region 2 has not been changed. The overall improved fit of predictions to data in Region 2 is the result of reduced mantle uplift that results from reducing the load in Region 1.

The best-fitting model from Regions 1 and 2 (i.e. unmodified in Region 3) underpredicts relative sea level at the Ottawa Islands and Inukjuak (Fig. 8). This version of the model also underpredicts early Holocene sea level fall at Deception Bay and Ungava Bay, although the model fits well the late Holocene history at both of these locations. The best-fitting model from Regions 1 and 2 also fits well the RSL data at Richmond Gulf. However, this model underpredicts present-day vertical uplift rates at all six GPS sites in Region 3 by 2–5 mm yr^{-1} (Fig. 9). The original ICE-5G model also underpredicts vertical motion rates in Region 3 by amounts similar to those of the starting best-fitting model of Regions 1 and 2.

To seek a better fit to the strongly underpredicted regional GPS data, as well as the underpredicted sea level change at the Ottawa Islands and Inukjuak, ice was thickened throughout Region 3. The addition of thicker ice increases the magnitude of all predictions of present-day uplift, and moves predictions at all sites but Kuujjuarapik to within or near the uncertainty of the measured rate (Fig. 9). The adjustment for the present-day mass loss effect is shown explicitly in Fig. 9, and reaches maximum values of approximately +0.6 to 0.8 mm yr^{-1} on Ungava Peninsula (Table 1). Although the magnitude of this effect is smaller than the uncertainty of the measured rates on Ungava Peninsula, its addition to the predicted rates for just the long-term GIA response improves the fit of the total predicted rates to the measured rates. When corrected for the present-day mass loss effect, the MSE misfit of the GPS data for the best-fitting model from Regions 1 and 2 (denoted R1 + R2) is MSE_{ave} (R1 + R2) = 5.2 mm^2 yr^{-2}, while the modified Region 3 (R3) model has a misfit of MSE_{ave} (R3) = 0.5 mm^2 yr^{-2}.

However, despite the much improved fit to the measured vertical uplift rates, thickened ice in this region does not significantly

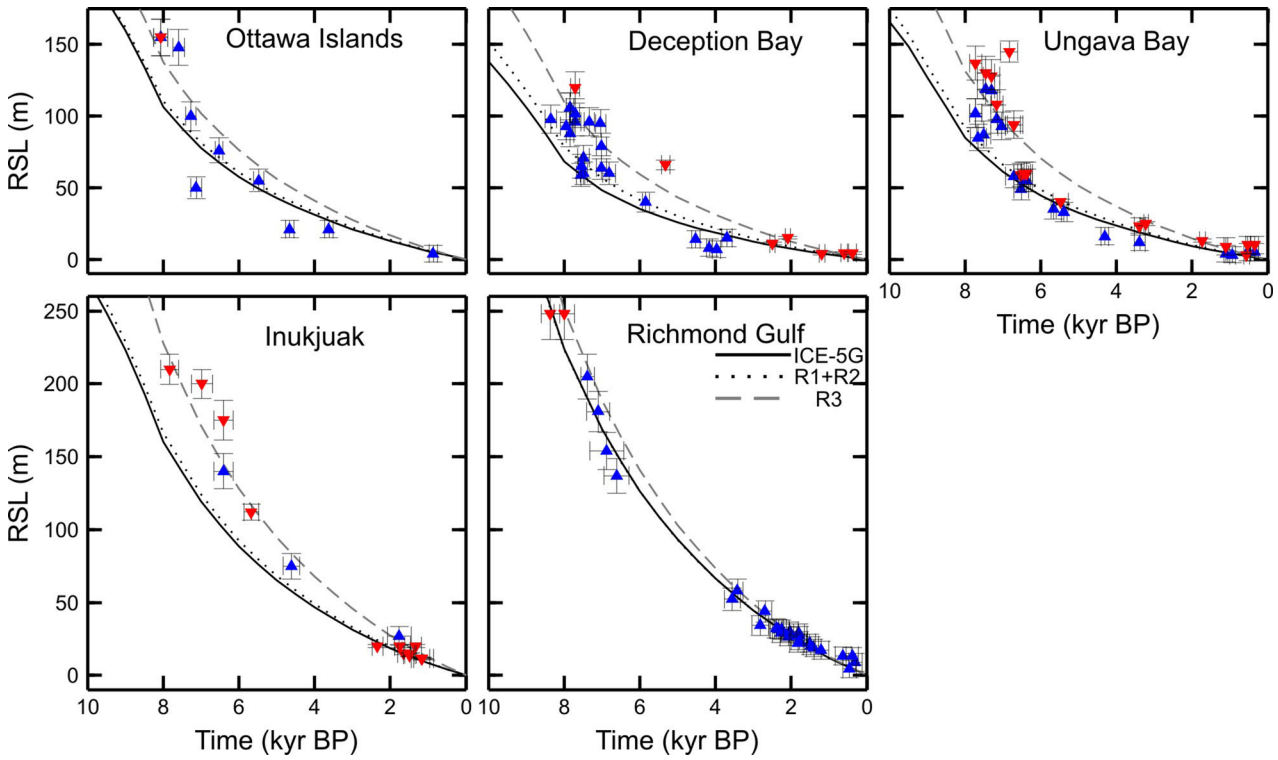

Figure 8. Relative sea level predictions and measurements for Region 3. Sea level measurements are plotted as described in the caption to Fig. 4. Both the original model and the best-fitting model from Regions 1 and 2 (solid black and dotted black lines, respectively) tend to underpredict the position of sea level at all locations except Richmond Gulf. An ice sheet reconstruction with thickened ice in Region 3 improves the fit of the predictions to the data from Inukjuak. For the Ottawa Islands and Deception and Ungava bays, the thickened reconstruction leads to better agreement in the early Holocene, but sea level is overpredicted in the mid- and late-Holocene (grey dashed line). All model predictions fit the data well at Richmond Gulf.

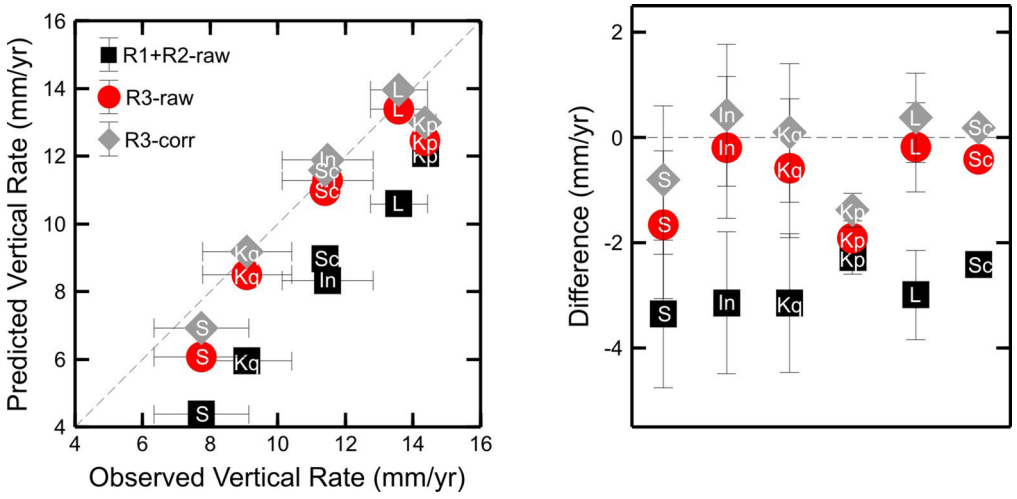

Figure 9. Predicted versus GPS-observed vertical rates of uplift in Region 3 (left-hand panel), and the differences between the predicted and observed rates (right-hand panel). The best-fitting model from Regions 1 and 2 (black squares, R1 + R2-raw) underpredicts rates of vertical uplift at all locations in Region 3. An ice sheet reconstruction with thickened ice in Region 3 improves the fit of the predictions to the data (red circles, R3-raw). The R1 + R2-raw and R3-raw predictions do not include the component of uplift resulting from present-day mass loss of Arctic glaciers and ice caps, and the Greenland Ice Sheet. The R3-corr predictions (grey diamonds) include the effect of present-day mass loss of the nearby ice cover. L, Laforge; In, Inukjuak; Kp, Kuujjuarapik; Kq, Kuujuak; S, Salluit; Sc, Schefferville.

improve the fit of the GIA model predictions to the RSL measurements with the exception of Inukjuak (Fig. 8). Relative to both the original ICE-5G and the R1 + R2 model, the fit at Deception Bay and Ungava Bay is improved for the early Holocene portion of the curves, and worsened for the late Holocene portion of the curves. The net result is that the model with thickened ice increases the overall χ^2 misfit of the predictions to the RSL data from both Deception and Ungava bays. At Ottawa Islands, the fit of the modified R3 model is also worsened (larger χ^2) relative to both ICE-5G and the R1 + R2 model. All versions of the ice sheet reconstruction maintain a good fit with the RSL data from the Richmond Gulf control site.

The RSL histories at Deception and Ungava bays both have discrepant or otherwise difficult to interpret ages, and the inability of either the starting model or the model developed for Region 3 to adequately fit the record of both early and late Holocene sea level change at these sites may indicate that separation of the data into more localized sea level histories is required. Alternatively, it is possible that an improved fit of the model to the RSL measurements from Deception and Ungava bays could be obtained by modifying the timing history in the ice sheet reconstruction to feature either more rapid initial deglaciation or a delayed onset of deglaciation, or by exploring regional variations to the selected earth model. It may, however, be difficult to find a GIA model that can simultaneously satisfy Deception and Ungava bays' late Holocene RSL histories, which imply relatively low rates of present-day uplift, and SALL and KUJQ's significantly larger observed vertical uplift rates from GPS.

Because of the differences between the sea level histories and the measured rates of current vertical uplift, it is difficult to assert a strong preference for thickening the ice model directly on Ungava Peninsula. However, GPS-measured uplift rates south of Ungava Peninsula (KUUJ, LFRG and SCH2) strongly support the addition of ice in more central regions of Quebec, and relative to ICE-5G, Argus & Peltier (2010) identified southern Quebec as a region where crustal uplift is significantly underpredicted. We therefore retain the version of the ice sheet reconstruction developed for Region 3 because (1) it provides a much better fit to all of the GPS data from the northern portion of the region, (2) there is uncertainty associated with interpretation of the RSL histories owing to discrepant or otherwise ambiguous ages and (3) it maintains regional continuity with the thicker ice in the southern portion of Region 3, where Argus & Peltier (2010) have also suggested thicker ice is needed.

4.3 Region 4

Region 4 includes Baffin Island, Foxe Basin and Melville Peninsula. The RSL histories examined in this region are from Igloolik, Cape Thalbitzer, Foxe Peninsula, Tikiraq River, Lavoie Point, Inugsuin Fiord, Iqaluit and Cape Tanfield (IGLO, THAL, FOXE, TIKI, LAVO, INUG, IQAL and TANF, respectively). This region is characterized by well constrained sea level histories, particularly on central and northern Baffin Island (Tikiraq River, Lavoie Point and Inugsuin Fiord). Foxe Peninsula has few RSL measurements, but represents the southernmost available data set from near Foxe Basin, a former load centre of the LIS. The sea level history at Cape Tanfield is well constrained overall, although there is a large gap in the data between ∼5 and 8 cal kyr BP. In Region 4 there are GPS-measured uplift rates from Igloolik and Qikiqtarjuak (IGLO, QIKI) and Iqaluit (IQAL, IQLU).

ICE-5G and the best-fitting model from Regions 1–3 reasonably predict the sea level record in the Foxe Basin area at Igloolik, Cape Thalbitzer and Foxe Peninsula, but overpredict sea level at Tikiraq River, Lavoie Point and Inugsuin Fiord (Fig. 10). At Iqaluit there is a more complex sea level history, including rapid initial emergence between 9 and 8 cal kyr BP. Because there are no marine measurements for Iqaluit after ∼7 cal kyr BP, the sea level record cannot constrain whether the rapid sea level fall was followed by continually decreasing emergence or a period of submergence. The starting model from Regions 1–3 underpredicts Iqaluit's early Holocene sea level high stand, but overpredicts sea level change after 8 cal kyr BP (Fig. 10). The present-day vertical uplift rates predicted by the model from Regions 1–3 tend to be underpredicted, although all predictions except that for QIKI are within or near the uncertainty of the measurements ('Q', Fig. 11).

To achieve a better fit between the model predictions and the Baffin Island RSL measurements, we reduce ice thicknesses across the island by factors ranging from 0.7 to 0.85. The ice coverage is not altered across Foxe Basin or Melville Peninsula because the fit of the model is already good in these locations. The reduced ice thicknesses result in significantly improved RSL predictions for all of the Baffin Island locations, except for Cape Tanfield, which is fit equally well by both models (Fig. 10). At Foxe Peninsula, the χ^2 misfit of the model predictions to the RSL measurements is increased only slightly by the thinned ice on Baffin Island.

Reducing ice thicknesses across Baffin Island reduces the predicted vertical uplift rates associated with the long-term GIA response at each of the GPS sites (Fig. 11). However, because Baffin Island has ice caps, and is also relatively close to the Greenland Ice Sheet, the estimated present-day ice mass loss effect on crustal motion for Region 4 is large (+1.1 to +2.9 mm yr^{-1}, Table 1). Fig. 11 shows the estimated vertical uplift rate adjustment for present-day ice mass loss. The effect is important for Region 4, and its addition to the predicted rates of uplift for the long-term GIA response helps to improve the fit of the R4 model predictions to the GPS data. When adjusted for the present-day mass loss effect, the R4 model has a misfit of MSE (R4) = 1.2 mm^2 yr^{-2}.

5 DISCUSSION

5.1 Regional contributions to the global sea level budget

The region-specific changes to the LGM ice thickness and global sea level equivalent of the cumulative best-fitting ice sheet reconstruction relative to the original ICE-5G model are shown in Figs 12 and 13. The values are calculated using the present-day ocean area. At up to −10.0 m of global sea level equivalent, the reduction to the ice thicknesses in Region 1 is the largest change to globally averaged sea level. This result is in part due to the fact that Region 1 is larger than any of the other regions (Fig. 1). Also, Region 1 had the largest original volume, and thus proportionally, the global sea level equivalent values are more sensitive to percentage load changes in Region 1 than in other regions. The thickened load in Region 3 contributes an additional +2.5 m to LGM globally averaged sea level, and the thinning of Region 4 contributes −0.4 m. The net change in global sea level equivalent at LGM for North America for the modified ice sheet reconstruction is approximately −7.9 m.

Differential vertical land motion rates predicted by the cumulative best-fitting ice sheet model and the original ICE-5G model were compared to the results of Argus & Peltier (2010) for ICE-5G for southern Canada (not shown). The comparison suggests that additional thinning to our ice model may still be required in Manitoba to obtain a good fit with GPS uplift rates. We have not added ice in the region of the northern British Columbia–Alberta border, although this area was identified by Argus & Peltier (2010) as an overly thin region in ICE-5G. However, it seems unlikely that a contribution from thicker ice here would exceed that obtained for Region 3, which was 2.5 m. It is possible that western Canada's contribution to globally averaged sea level may be further increased by thickening the ice model over parts of the Cordilleran Ice Sheet, and along the western margins of the LIS, as appears to have occurred for ICE-6G.

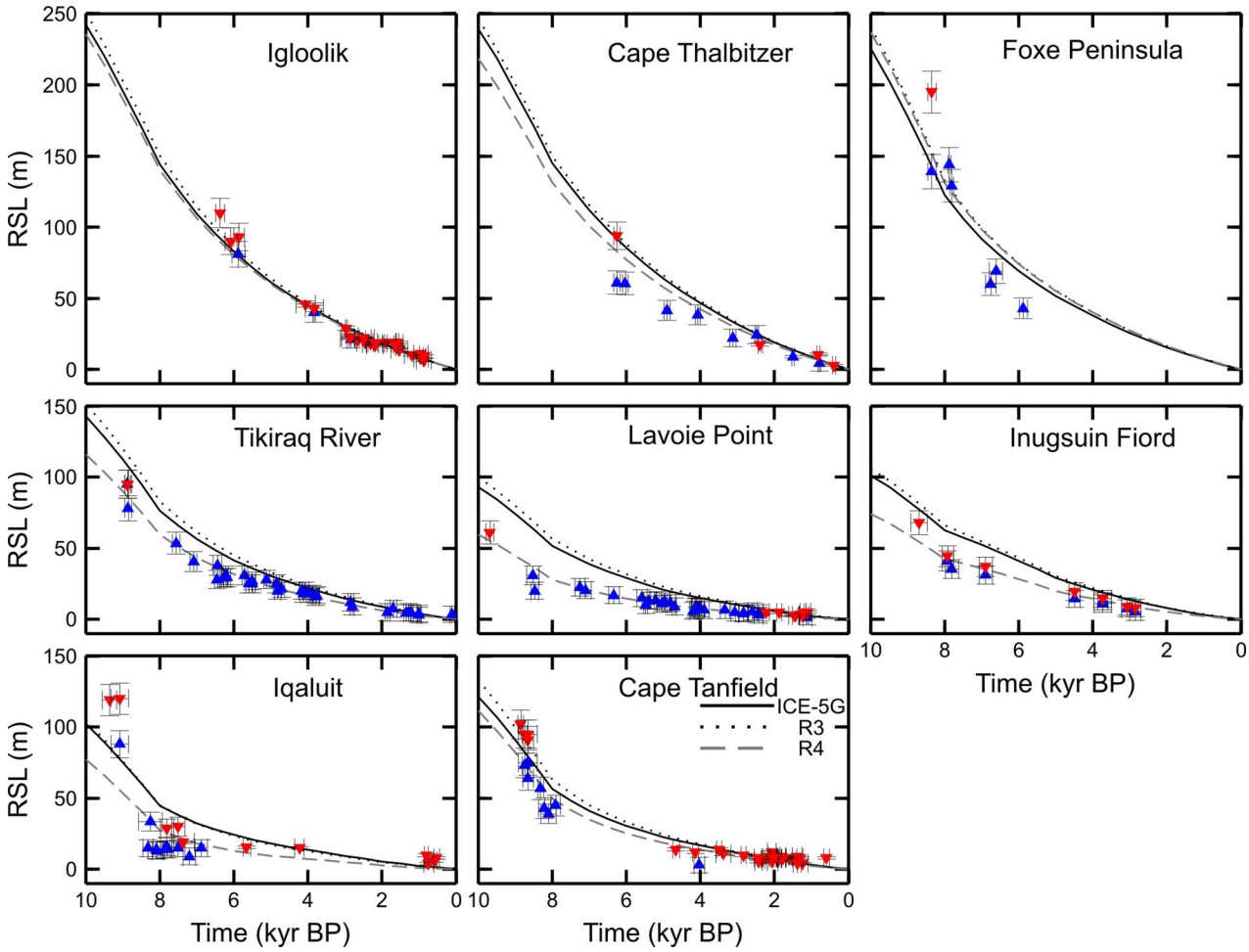

Figure 10. Relative sea level predictions and measurements for Region 4. Sea level measurements are plotted as described in the caption to Fig. 4. Both the original model and the best-fitting model from Region 3 (solid black and dotted black lines, respectively) well predict sea level in the Foxe Basin region (top panel), but overpredict sea level on northern Baffin Island (middle panel) and at Iqaluit. An ice sheet reconstruction with thinned ice on Baffin Island improves the fit of the predictions to the data on northern Baffin Island and at Iqaluit, and maintains a good fit to the data from around Foxe Basin and Cape Tanfield (grey dashed line).

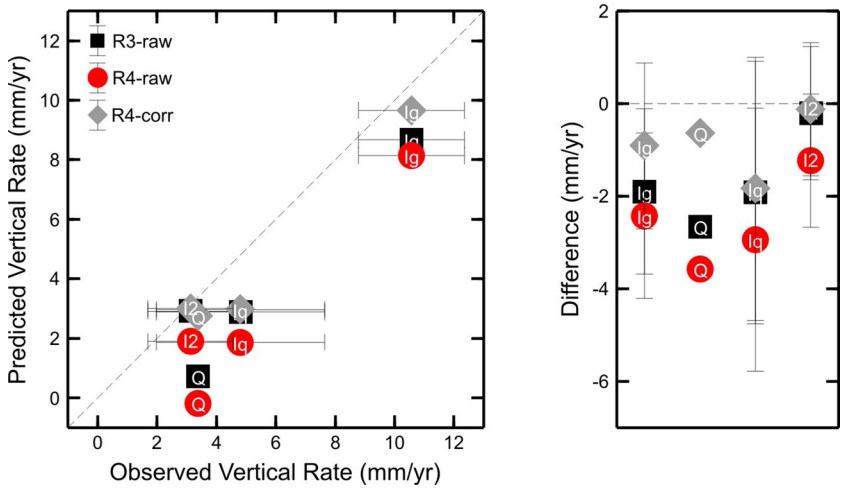

Figure 11. Predicted versus GPS-observed vertical rates of uplift in Region 4 (left-hand panel), and the differences between the predicted and observed rates (right-hand panel). The best-fitting model from Region 3 (black squares, R3-raw) underpredicts rates of vertical uplift at all locations in Region 4. An ice sheet reconstruction with thinned ice in Region 4 worsens the fit of the predictions to the data (red circles, R4-raw). The R3-raw and R4-raw predictions do not include the component of uplift resulting from present-day mass loss of Arctic glaciers and ice caps, and the Greenland Ice Sheet. When adjusted for this effect (grey diamonds, R4-corr) the fit of the predicted rates to the observed rates is significantly improved. Ig, Igloolik; Iq, Iqaluit (site IQAL); I2, Iqaluit (site IQLU); Q, Qikiqtarjuak.

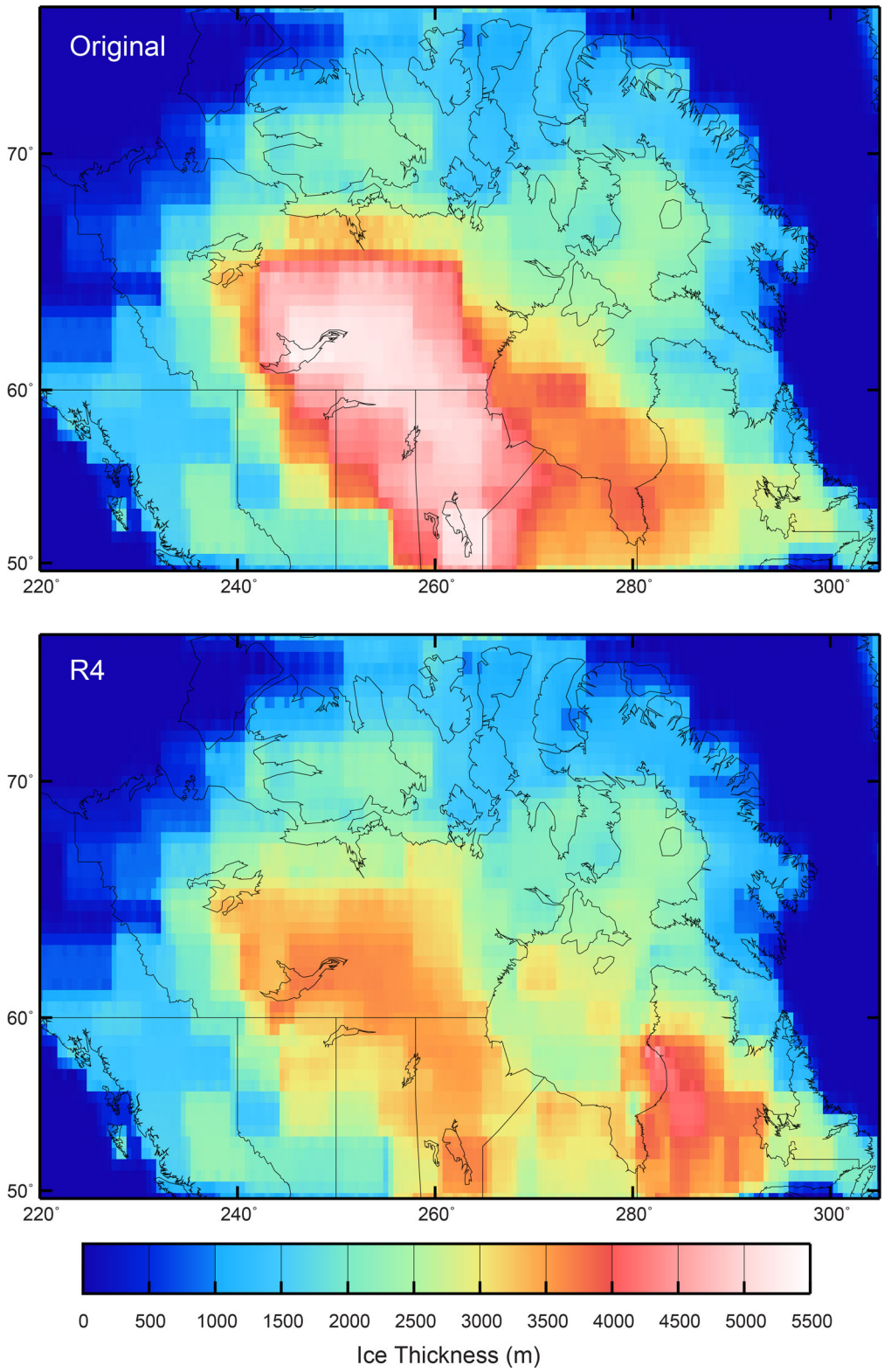

Figure 12. Last glacial maximum ice thicknesses of the original ice sheet reconstruction (top panel) and the best-fitting (R4, also termed Laur16) ice sheet reconstruction (bottom panel).

Because ICE-5G satisfies the far-field sea level low stand of ∼120–125 m inferred from Barbados RSL data (Fairbanks 1989; Peltier & Fairbanks 2006), reducing North America's contribution to globally averaged sea level at the LGM by 7.9 m introduces a deficit to the global sea level budget that must be offset by adding ice elsewhere in the global model. Furthermore, Austermann *et al.* (2013) have suggested that fitting the Barbados RSL data requires an LGM eustatic low stand of ∼130 m, a value consistent with far-field sea level records from other locations (Yokoyama *et al.* 2000). A 130 m eustatic value would further increase the deficit

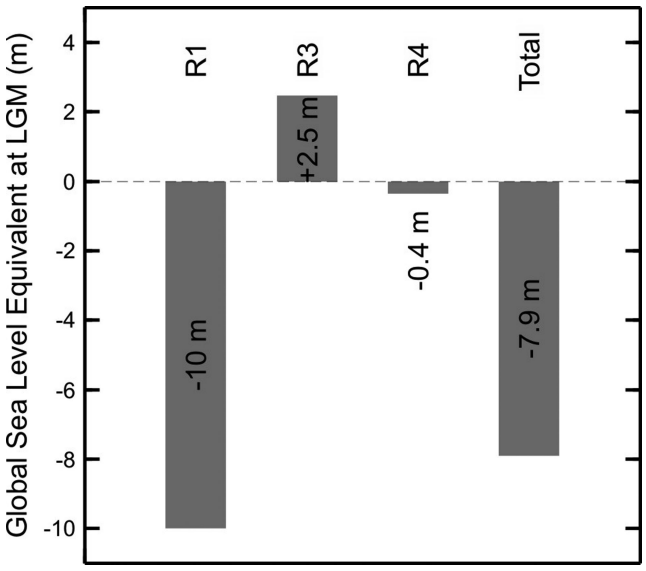

Figure 13. Calculated LGM global equivalent sea level changes that result from the ice sheet reconstruction modifications in Regions 1, 3 and 4 (no changes were made to the ice load in Region 2).

to globally averaged sea level, as do recent estimates of Antarctica's contribution to the global sea level budget. In ICE-5G, the global sea level equivalent contribution of Antarctica is ∼17–18 m. This value is in excess of current estimates of ∼8–11 m derived from Antarctic ice sheet reconstructions developed to incorporate recent glacial-geological and geodetic constraints (Ivins & James 2005; Whitehouse *et al*. 2012; Ivins *et al*. 2013). Thus, decreased Antarctic ice volume and increased LGM eustatic estimates both suggest that the global sea level deficit may be even larger than the amount derived here for North America. The results of this study are therefore compatible with Austermann *et al*.'s (2013) suggestion that a significant portion of Northern Hemisphere ice may not be accounted for by current ice models, and further indicate it may be challenging to place a large volume of this ice within the LIS.

5.2 Summary of Laurentide Ice Sheet reconstruction results

In Fig. 14, the RSL χ^2 misfit values and GPS predictions of the original ICE-5G reconstruction are compared to those of Laur16. The χ^2 misfit value for all RSL measurements is reduced from 21.0 for the original model to 9.1 for Laur16. The MSE misfit value for all GPS measurements is reduced from 9.0 mm^2 yr^{-2} for the original model to 1.0 mm^2 yr^{-2} for Laur16. Region 1 shows the most significant improvement, although Regions 2 and 4 are also improved. As discussed in Section 4.2, Region 3 represents the only region for which clear improvement to the fit of the RSL data was not achieved.

The results of the sensitivity analysis in Regions 1 and 2 are in accordance with studies that have suggested a misfit between ICE-5G and data constraints within North America (Braun *et al*. 2008; van der Wal *et al*., 2008, 2010; Wang *et al*. 2013), and further agree with the conclusions of Lambert *et al*. (2006), Argus & Peltier (2010), Mazzotti *et al*. (2011) and Peltier *et al*. (2015) that the ice sheet thickness in ICE-5G is too large in Region 1. A uniform 30 per cent reduction to the load thickness in Region 1 minimizes the misfit to most of the Holocene relative sea level data as well as the observed present-day uplift rates.

The ∼30 per cent load reduction in Region 1 simultaneously improves the fit of the model to the RSL data in Region 2. In Region 2, no version of the ice sheet reconstruction is able to reproduce the rapid fall in sea level observed at Murray Bay at 10 kyr BP. This sharp drop in sea level may indicate a localized region where more rapid deglaciation took place relative to that prescribed by the timing history of the ice sheet model. Alternatively, the rapid initial emergence at Murray Bay may reflect tectonic movement along faults of the Boothia Arch that became reactivated in the

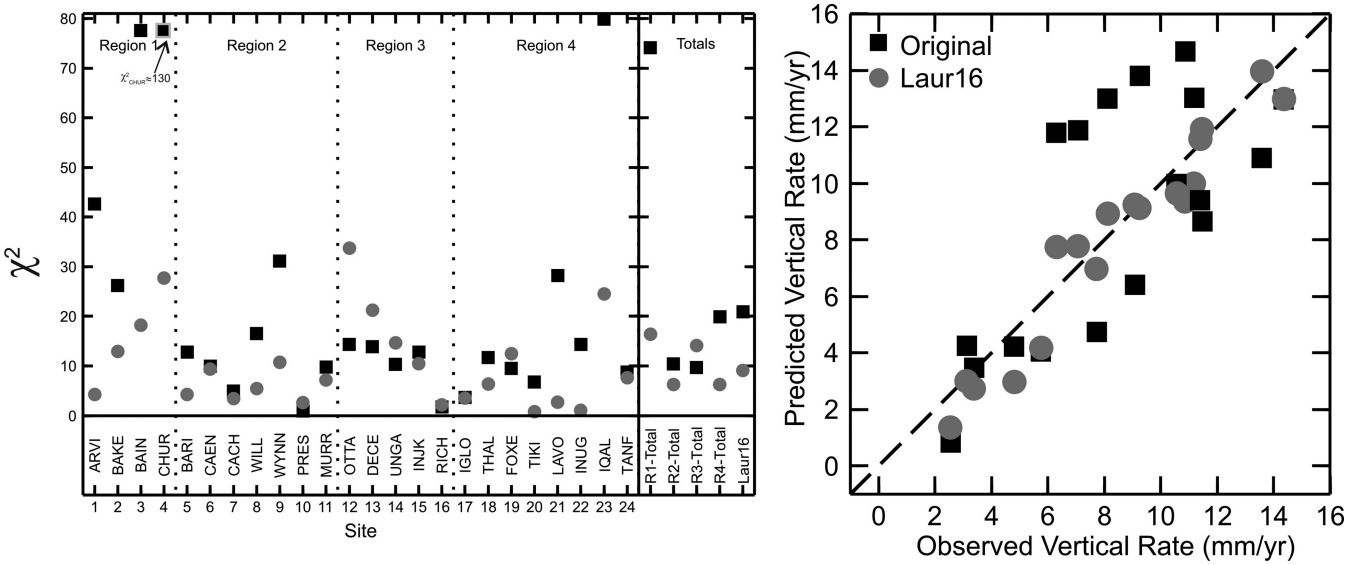

Figure 14. Summary of the fit of the original ice sheet reconstruction (black squares) and the best-fitting ice sheet reconstruction (grey circles, Laur16) to all RSL and GPS measurements in Regions 1–4. The left panel shows the χ^2 misfit values for each of the individual RSL sites, as well as the cumulative χ^2 misfit values for each region (R1-Total, R2-Total, R3-Total and R4-Total) and all regions (Laur16). The overall χ^2 misfit value on the RSL data decreases from 21.0 for the starting model to 9.1 for the best-fitting Laur16 model. Note that the χ^2 misfit value at Churchill plots off the vertical scale (at approximately 130). The right panel shows the predicted versus observed vertical uplift rates for the original model (black squares) and the Laur16 model (grey circles) for all 18 GPS sites. The overall MSE misfit value on the GPS data decreases from 9.0 mm^2 yr^{-2} for the starting model to 1.0 mm^2 yr^{-2} for Laur16.

early Holocene by crustal uplift associated with deglaciation (Dyke *et al*. 1991).

In Region 3, compared to a model with thickened ice, the original ICE-5G model better predicts regional sea level change in northern Quebec in the χ^2 sense, but strongly underpredicts all six regional GPS-measured uplift rates. In particular, it is challenging to reconcile late Holocene RSL change and present-day vertical uplift observations from Ungava Peninsula. The sea level histories of Deception and Ungava bays imply present-day rates of crustal uplift that appear significantly smaller than those observed by the nearest continuous GPS sites. The uplift rate inferred by Inukjuak's RSL curve is, however, large (Gray *et al*. 1993) and is in general agreement with the large GPS-measured uplift rate at INJK. Also, south of Ungava Peninsula, a thickened ice sheet reconstruction is strongly supported by the GPS-measured present-day uplift rates at KUUJ, LFRG and SCH2. This result is also consistent with the suggestion of Argus & Peltier (2010) that GPS-measured rates of vertical uplift indicate that more ice can be added to ICE-5G in southern and eastern Quebec. It is less clear, however, whether the ice model should be thickened into northernmost Quebec. Predicted rates of vertical uplift on Ungava Peninsula are moderately sensitive to the present-day mass loss of Greenland and Baffin Island. A higher rate of assumed mass loss for either of these locations would further increase predicted rates of vertical uplift and simultaneously reduce the magnitude of ice model thickening needed on Ungava Peninsula.

In Region 4, a reduction of ∼15–25 per cent to ICE-5G ice thicknesses across Baffin Island improves the fit of the model to the regional RSL measurements. This reduction corresponds to a modest decrease in peak ice thickness from approximately 1.6 km to between 1.2 and 1.35 km. However, this model does not reproduce the sharp fall in relative sea level observed at Iqaluit between 9 and 8 cal kyr BP. This result suggests that a combination of locally thicker ice prior to 9 cal kyr BP and more rapid initial deglaciation may be required in the ice model.

Due to the presence of ice caps and the nearby Greenland Ice Sheet, it is important in Region 4 to include the elastic effect of present-day ice mass change on GPS observations. Inclusion of this effect significantly improves the fit of model predictions to measurements. At QIKI, the estimated present-day mass loss effect is particularly large (2.9 mm yr^{-1}) and corresponds to approximately 85 per cent of QIKI's total observed rate of 3.4 mm yr^{-1} (Table 1). QIKI is strongly influenced by the observed rapid present-day mass loss of the nearby Penny Ice Cap on the southeast coast of Baffin Island (Gardner *et al*. 2011; Zdanowicz *et al*. 2012). The ice caps have coarse spatial resolution in the model grid, and the assumed mass loss rates are uncertain. Therefore, the calculated vertical crustal motion due to present-day mass loss rates is preliminary. In addition, measured vertical uplift rates may be significantly influenced by Neoglacial volume changes to the ice caps, although this effect has not yet been explored for the study area.

Recent updates to LIS margin chronology suggest that ice in the western Canadian Arctic Archipelago (Lakeman & England 2013) and on northeastern Baffin Island (Briner *et al*. 2005) was more extensive at LGM than depicted in the margin chronology used in this study (from Dyke *et al*. 2003). Our study regions largely lie to the east and south of the areas with a revised margin chronology. It is possible that changes to the loading history and ice sheet margins in these locations could modestly influence predicted RSL change in Region 2 and at Inugsuin Fiord, respectively. However, it is unlikely that incorporation of these revisions to margin chronology would significantly impact estimates of the LGM global sea level equivalent of Laur16.

5.3 Comparison of Laur16 to ICE-6G

Recently, Peltier *et al*. (2015) presented an update to the North American component of ICE-5G and ICE-6G. Here, we briefly compare the predictions of ICE-6G to our final model, termed Laur16 (details of the comparison are given in the supporting information). Generally, both ICE-6G and Laur16 have thinner ice west of Hudson Bay (and provide a significantly better fit to RSL data), and thicker ice east of Hudson Bay, than ICE-5G. Relative to Laur16, ICE-6G LGM ice thicknesses are: (i) less thinned within and directly west of Hudson Bay, (ii) thicker in northern Alberta and parts of the westernmost LIS, (iii) less thinned in eastern Hudson Bay and around James Bay and (iv) thicker in Foxe Basin and Baffin Island. Within the study region, the ICE-6G model overall shows less volume change relative to ICE-5G than Laur16. In Region 1 (within western Hudson Bay, and west of Hudson Bay) the net LGM load reduction is approximately −6 m; the load also appears thickened farther west, within the westernmost LIS. Conversely, ICE-6G has up to ∼3.5 m more global sea level equivalent than ICE-5G in Region 3 (within eastern Hudson Bay and Quebec) and up to ∼2 m more in Region 4 (Baffin Island and Foxe Basin). Thicker ice in the westernmost LIS however may not be supported by the regional glacial history, which indicates the peak extent of the Cordilleran Ice Sheet was not reached until after the LGM of the LIS (Dyke *et al*. 2002), and likewise not in Region 4, where the RSL data do not suggest a need for thicker ice (Figs 10 and S4).

The cumulative χ^2 value for the 24 RSL histories used in this study is approximately 9 for Laur16 and approximately 18 for ICE-6G, indicating a factor-of-two better fit for Laur16. The total MSE misfit value for the 18 GPS measurements used in this study is 1.0 mm^2 yr^{-2} for Laur16 and 1.6 mm^2 yr^{-2} for ICE-6G, indicating a slightly better fit for Laur16. Although partly because the model was designed specifically to fit data from northern Canada, Laur16 better reproduces both types of GIA-related measurements within the study area.

6 CONCLUSIONS

An improved GIA model, termed Laur16, is developed here by sequentially scaling the ice load thickness history for four regions of an area encompassing much of the northern Laurentide Ice Sheet (Fig. 2). The starting model is ICE-5G (Peltier 2004) and the final model provides an improved fit to selected RSL histories and GPS-constrained vertical land motion in the area. Compared to ICE-6G (Peltier *et al*. 2015), Laur16 also provides an improved fit (about a factor of 2 χ^2 reduction) to RSL histories and a slightly improved fit (about a factor of 1.6 MSE reduction) to GPS uplift rates within the study area. For the region west of Hudson Bay, the fit of GIA model predictions to four relative sea level histories and six present-day rates of vertical motion indicates that the former Laurentide Ice Sheet reached a maximum thickness of ∼3.4–3.6 km here. This result is generally compatible with the configuration of the ICE-6G model which indicates thicknesses of ∼3.5 km in this region (Peltier *et al*. 2015) and with the 1.5 km thickness reduction to ICE-5G in central Canada indicated by Vettoretti & Peltier (2013). The reduction to the load history in Region 1 also increases the predicted position of sea level in load-marginal regions, which improves the

fit of model predictions to RSL data in a broad region to the north of the central LIS.

Conversely, relative sea level data and present-day vertical uplift rates from northern and central Quebec support a thicker ice sheet, locally up to ~4 km thick. A model with ice thickened in this region decreases the MSE misfit of six continuous GPS sites in northern and central Quebec; however the χ^2 misfit to the RSL data is slightly worsened. No version of the GIA model explored in this study is able to simultaneously reproduce the rapid initial emergence and the slower rate of late Holocene emergence inferred by the RSL data from Ungava Peninsula. Peltier *et al*. (2015) also note that ICE-6G provides a poorer fit to RSL change at Deception and Ungava bays than ICE-5G. The net outcome of fitting the GIA model predictions to the regional RSL and GPS measurements indicates a preference for a thickened ice sheet reconstruction in Region 3, although the complex record of RSL change on Ungava Peninsula suggests that considering more localized changes to the ice sheet history and margin chronology here may be worthwhile.

In Region 4, the fit of the original ICE-5G model to the RSL data is generally good in the former load centre of Foxe Basin. Modest thinning (by approximately ≤300 m) to the ice sheet history on Baffin Island results in an improved fit to measurements of RSL, particularly on northern Baffin Island, and corresponds to peak regional thicknesses of approximately 1.3 km. When adjusted for the estimated effect of present-day ice mass loss, the rates of vertical uplift predicted by the model in Region 4 also have a reasonable fit to the GPS-measured rates. Therefore, the inclusion of the present-day ice loss effect allows predictions from a thinner ice sheet reconstruction in Region 4 (which better fit measurements of Holocene RSL change) to be reconciled with the measured vertical uplift rates.

Relative to ICE-5G and ICE-6G, the final Laur16 model reduces the overall χ^2 misfit to 24 RSL histories by at least a factor of 2, and relative to ICE-5G, reduces the overall MSE misfit to 18 GPS measurements by a factor of 9.The net change to global sea level equivalent at LGM of the final model is approximately −8 m, although this value may be partially offset by thickening the ice sheet model in regions of western Canada, a modification included in ICE-6G (Peltier *et al*. 2015) but not incorporated here. Future work could consider further these regional differences in the model-predicted LGM ice volume, and their role in constraining the North American contribution to global sea level and the balancing of the global sea level budget (e.g. Austermann *et al*. 2013).

The ice sheet history developed here is dependent on the assumed earth model and VM5a viscosity profile. Additional study could also examine the sensitivity of this model to changes in mantle viscosity and lithospheric thickness. As well, spatially denser coverage by continuous GPS sites in the north (e.g. Wu *et al*. 2010), as well as longer observation times leading to reduced uncertainty of measurements of vertical uplift, will better constrain regional trends of present-day crustal uplift and thus benefit glacial isostatic adjustment studies. Gravity change measurements likewise can aid in the determination of the relative thickness and spatial geometry of the former Laurentide Ice Sheet (e.g. Lambert *et al*. 2006; Steffen *et al*. 2012). However, relative sea level measurements will continue to provide fundamental constraints on GIA models in northern Canada because they provide a record of sea level change through time, while vertical motion observations from GPS only provide a snapshot of present-day rates. The Laur16 model presented here, together with the companion SJD15 Innuitian Ice Sheet model (Simon *et al*. 2015), provides updated constraints on ice sheet thickness history and updated predictions of relative sea level and vertical land motion having potential applications for a dynamic geodetic reference frame, for projections of future sea level change, for predictions of intraplate crustal deformation, and as a foundation for future investigations of GIA in northern Canada.

ACKNOWLEDGEMENTS

This work was supported by the ArcticNet Network of Centres of Excellence, the Nunavut Climate Change Partnership, and the Earth Sciences Sector (ESS) Climate Change Geoscience Program (CCGP). KMS was supported by the ArcticNet Network of Centres of Excellence, the University of Victoria, and the ESS CCGP. We thank Felicity Rhone for assistance with the model calculations and figures for the supporting information. We thank Jan Bednarski, Jerry Mitrovica and two anonymous reviewers for careful reviews which substantially improved the manuscript. This is ESS contribution number 20150224.

REFERENCES

Altamimi, Z., Collilieux, X. & Métivier, L., 2011. ITRF2008: an improved solution of the international terrestrial reference frame, *J. Geod.,* **85,** 457–473.

Argus, D.F. & Peltier, W.R., 2010. Constraining models of postglacial rebound using space geodesy: a detailed assessment of model ICE-5G (VM2) and its relatives, *Geophys. J. Int.,* **181,** 697–723.

Argus, D.F., Peltier, W.R., Drummond, R. & Moore, A.W., 2014. The Antarctica component of postglacial rebound model ICE-6G_C (VM5a) based upon GPS positioning, exposure age dating of ice thicknesses, and relative sea level histories, *Geophys. J. Int.,* **198,** 537–563.

Austermann, J., Mitrovica, J.X., Latychev, K. & Milne, G.A., 2013. Barbados-based estimate of ice volume at Last Glacial Maximum affected by subducted plate, *Nat. Geosci.,* **6,** 553–557.

Bolch, T., Sørensen, L.S., Simonsen, S.B., Mölg, N., Machguth, H., Rastner, P. & Paul, F., 2013. Mass loss of Greenland's glaciers and ice caps 2003–2008 revealed from ICESat laser altimetry data, *Geophys. Res. Lett.,* **40,** 1–7.

Braun, A., Kuo, C.-Y., Shum, C.K., Wu, P., van der Wal, W. & Fotopoulos, G., 2008. Glacial isostatic adjustment at the Laurentide ice sheet margin: models and observations in the Great Lakes region, *J. Geodyn.,* **46,** 165–173.

Briner, J.P., Miller, G.H., Davis, P.T. & Finkel, R.C., 2005. Cosmogenic exposure dating in arctic glacial landscapes: implications for the glacial history of northeastern Baffin Island, Arctic Canada, *Can. J. Earth Sci.,* **42,** 67–84.

Craymer, M.R., Henton, J., Piraszewski, M. & Lapelle, E., 2011. An updated GPS velocity field for Canada, *EOS, Trans. Am. geophys. Un.,* **92**(51), Fall Meeting Supplement, Abstract G21A-0793.

Dach, R. *et al.*, 2007. *Bernese GPS Software Version 5.0*, Astronomical Institute, University of Bern.

Dyke, A.S., 2004. An outline of North American deglaciation with emphasis on central and northern Canada, in *Quaternary Glaciations - Extent and Chronology, Part II. North America, Developments in Quaternary Science 2,* pp. 373–424, eds Ehlers, J. & Gibbard, P.L., Elsevier.

Dyke, A.S., Dredge, L.A. & Vincent, J-S., 1982. Configuration and dynamics of the Laurentide Ice Sheet during the Late Wisconsin maximum, *Géographie physique et Quaternaire,* **36,** 5–14.

Dyke, A.S., Morris, T.F. & Green, D.E.C., 1991. Postglacial tectonic and sea level history of the central Canadian Arctic, Bulletin 397, Geological Survey of Canada, Ottawa, pp. 1–56.

Dyke, A.S., Andrews, J.T., Clark, P.U., England, J.H., Miller, G.H., Shaw, J. & Veillette, J.J., 2002. The Laurentide and Innuitian ice sheets during the Last Glacial Maximum, *Quat. Sci. Rev.,* **21,** 9–31.

Dyke, A.S., Moore, A. & Robertson, L., 2003. Deglaciation of North America. Thirty-two digital maps at 1:7 000 000 scale with accompanying

digital chronological database and one poster (two sheets) with full map series, *Open File, 1574,* Geological Survey of Canada.

Dziewonski, A.M. & Anderson, D.L., 1981. Preliminary reference Earth model, *Phys. Earth planet. Inter.,* **25,** 297–356.

Engelhart, S.E., Peltier, W.R. & Horton, B.P., 2011. Holocene relative sea-level changes and glacial isostatic adjustment of the U.S. Atlantic coast, *Geology,* **39,** 751–754.

Fairbanks, R.G., 1989. A 17 000-year glacio-eustatic sea level record: influence of glacial melting rates on the Younger Dryas event and deep-ocean circulation, *Nature,* **342,** 637–642.

Gardner, A.S. *et al.*, 2011. Sharply increased mass loss from glaciers and ice caps in the Canadian Arctic Archipelago, *Nature,* **473,** 357–360.

Gardner, A.S. *et al.*, 2013. A reconciled estimate of glacier contributions to sea level rise: 2003 to 2009, *Science,* **340,** 852–857.

Gray, J., Lauriol, B., Bruneau, D. & Ricard, J., 1993. Postglacial emergence of Ungava Peninsula, and its relationship to glacial history, *Can. J. Earth Sci.,* **30,** 1676–1696.

Hughen, K.A. *et al.*, 2004. Marine04 Marine radiocarbon age calibration, 26 - 0 ka BP, *Radiocarbon,* **46,** 1059–1086.

Ivins, E.R. & James, T.S., 2005. Antarctic glacial isostatic adjustment: a new assessment, *Antarct. Sci.,* **17,** 541–553.

Ivins, E.R., James, T.S., Wahr, J., Schrama, E.J.O., Landerer, F.W. & Simon, K.M., 2013. Antarctic contribution to sea level rise observed by GRACE with improved GIA correction, *J. geophys. Res.,* **118,** 1–16.

Kendall, R.A., Mitrovica, J.X. & Milne, G.A., 2005. On post-glacial sea level – II. Numerical formulation and comparative results on spherically symmetric models, *Geophys. J. Int.,* **161,** 679–706.

Lakeman, T.R. & England, J.H., 2013. Late Wisconsinan glaciation and postglacial relative sea-level change on western Banks Island, Canadian Arctic Archipelago, *Quatern. Res.,* **80,** 99–112.

Lambert, A., Courtier, N. & James, T.S., 2006. Long-term monitoring by absolute gravimetry: tides to postglacial rebound, *J. Geodyn.,* **41,** 307–317.

Mazzotti, S., Lambert, A., Henton, J., James, T.S. & Courtier, N., 2011. Absolute gravity calibration of GPS velocities and glacial isostatic adjustment in midcontinent North America, *Geophys. Res. Lett.,* **38,** doi:10.1029/2011GL049846.

McNeely, R., Dyke, A.S. & Southon, J.R., 2006. Canadian marine reservoir ages, preliminary data assessment, Open file 5049, Geological Survey of Canada, Ottawa.

Mitrovica, J.X. & Milne, G.A., 2003. On post-glacial sea level: I. General theory, *Geophys. J. Int.,* **154,** 253–267.

Mitrovica, J.X. & Peltier, W.R., 1991. On postglacial geoid subsidence over the equatorial oceans, *J. geophys. Res.,* **96,** 20 053–20 071.

Mitrovica, J.X., Davis, J.L. & Shapiro, I.I., 1994. A spectral formalism for computing three-dimensional deformations due to surface loads, 1. Theory, *J. geophys. Res.,* **99,** 7057–7073.

Mitrovica, J.X., Forte, A.M. & Simons, M., 2000. A reappraisal of postglacial decay times from Richmond Gulf and James Bay, Canada, *Geophys. J. Int.,* **142,** 783–800.

Paulson, A., Zhong, S. & Wahr, J., 2007. Inference of mantle viscosity from GRACE and relative sea level data, *Geophys. J. Int.,* **171,** 497–508.

Peltier, W.R., 1994. Ice age paleotopography, *Science,* **265,** 195–201.

Peltier, W.R., 1996. Mantle viscosity and ice-age ice sheet topography, *Science,* **273,** 1359–1364.

Peltier, W.R., 1998. Postglacial variations in the level of the sea: implications for climate dynamics and solid-earth geophysics, *Rev. Geophys.,* **36,** 603–689.

Peltier, W.R., 2004. Global glacial isostasy and the surface of the ice-age Earth: the ICE-5G (VM2) model and GRACE, *Annu. Rev. Earth. planet. Sci.,* **32,** 111–149.

Peltier, W.R. & Drummond, R., 2008. Rheological stratification of the lithosphere: a direct inference based upon the geodetically observed pattern of the glacial isostatic adjustment of the North American continent, *Geophys. Res. Lett.,* **35,** doi:10.1029/2008GL034586.

Peltier, W.R. & Fairbanks, R.G., 2006. Global glacial ice volume and Last Glacial Maximum duration from an extended Barbados sea level record, *Quat. Sci. Rev.,* **25,** 3322–3337.

Peltier, W.R., Argus, D.F. & Drummond, R., 2015. Space geodesy constrains ice-age terminal deglaciation: the global ICE-6G_C (VM5a) model, *J. geophys. Res.,* **120,** 450–487.

Reimer, P.J. *et al.*, 2004. IntCal04 Terrestrial radiocarbon age calibration, 26 - 0 ka BP, *Radiocarbon,* **46,** 1029–1058.

Rignot, E., Velicogna, I., van den Broeke, M.R., Monaghan, A. & Lenaerts, J.T.M., 2011. Acceleration of the contribution of the Greenland and Antarctic ice sheets to sea level rise, *Geophys. Res. Lett.,* **38,** doi:10.1029/2011GL046583.

Shennan, I., 2007. Sea level studies: overview, in *Encyclopedia of Quaternary Science,* pp. 2967–2974, ed. Elias, S.A., Elsevier.

Shepherd, A. *et al.*, 2012. A reconciled estimate of ice-sheet mass balance, *Science,* **338,** 1183–1189.

Simon, K.M., 2014. Improved glacial isostatic adjustment models for northern Canada, *PhD thesis,* University of Victoria, Victoria, Canada.

Simon, K.M., James, T.S., Forbes, D.L., Telka, A.M., Dyke, A.S. & Henton, J.A., 2014. A relative sea-level history for Arviat, Nunavut, and implications for Laurentide Ice Sheet thickness west of Hudson Bay, *Quatern. Res.,* **82,** 185–197.

Simon, K.M., James, T.S. & Dyke, A.S., 2015. A new glacial isostatic adjustment model of the Innuitian Ice Sheet, Arctic Canada, *Quat. Sci. Rev.,* **119,** 11–21.

Steffen, H., Wu, P. & Wang, H., 2012. Optimal locations for absolute gravity measurements and sensitivity of GRACE observations for constraining glacial isostatic adjustment on the northern hemisphere, *Geophys. J. Int.,* **190,** 1483–1494.

Stuiver, M. & Polach, H.A., 1977. Discussion: reporting of ^{14}C data, *Radiocarbon,* **19,** 355–363.

Stuiver, M. & Reimer, P.J., 1993. Extended ^{14}C database and revised CALIB 3.0 ^{14}C age calibration program, *Radiocarbon,* **35,** 215–230.

Toscano, M.A., Peltier, W.R. & Drummond, R., 2011. ICE-5G and ICE-6G models of postglacial relative sea-level history applied to the Holocene coral reef record of northeastern St Croix, U.S.V.I.: investigating the influence of rotational feedback on GIA processes at tropical latitudes, *Quat. Sci. Rev.,* **30,** 3032–3042.

Van der Wal, W., Wu, P., Sideris, M.G. & Shum, C.K., 2008. Use of GRACE determined secular gravity rates for glacial isostatic adjustment studies in North-America, *J. Geodyn.,* **46,** 144–154.

Van der Wal, W., Wu, P., Wang, H. & Sideris, M.G., 2010. Sea levels and uplift rate from composite rheology in glacial isostatic adjustment modelling, *J. Geodyn.,* **50,** 38–48.

Vettoretti, G. & Peltier, W.R., 2013. Last Glacial Maximum ice sheet impacts on North Atlantic climate variability: the importance of a sea ice lid, *Geophys. Res. Lett.,* **40,** 6378–6383.

Walcott, R.I., 1972. Late Quaternary vertical movements in eastern North America: quantitative evidence of glacio-isostatic rebound, *Rev. Geophys. Space Phys.,* **10,** 849–884.

Wang, H. *et al.*, 2013. Increased water storage in North America and Scandinavia from GRACE gravity data, *Nat. Geosci.,* **6,** 38–42.

Whitehouse, P.L., Bentley, M.J., Milne, G.A., King, M.A. & Thomas, I.D., 2012. A new glacial isostatic adjustment model for Antarctica: calibrated and tested using observations of relative sea-level change and present-day uplift rates, *J. geophys. Res.,* **190,** 1464–1482.

Wu, P., Steffen, H. & Wang, H., 2010. Optimal locations for GPS measurements in North America and northern Europe for constraining glacial isostatic adjustment, *Geophys. J. Int.,* **181,** 653–664.

Yokoyama, Y., Lambeck, K., De Deckker, P., Johnston, P. & Fifield, L.K., 2000. Timing of the Last Glacial Maximum from observed sea-level minima, *Nature,* **406,** 713–716.

Zdanowicz, C., Smetny-Sowa, A., Fisher, D., Schaffer, N., Copland, L., Eley, J. & Dupont, F., 2012. Summer melt rates on Penny Ice Cap, Baffin Island: past and recent trends and implications for regional climate, *J. geophys. Res.,* **117,** doi:10.1029/2011JF002248.

SUPPORTING INFORMATION

Additional Supporting Information may be found in the online version of this paper:

Figure S1. Region 1 relative sea level measurements and predictions for ICE-5G (black line), Laur16 (also called R4, grey dashed line), and ICE-6G (blue line). Lower observational constraints are shown by blue triangles; sea level was at or above these points. Upper observational constraints are shown by red triangles; sea level was at or below these points. Triangles point in the direction of the inferred position of sea level. The curves for ICE-6G are cut-off at the time at which the presence of nearby ice in the palaeotopography field begins to contaminate the derived RSL curve; only the RSL data that are present after these cut-off times are shown or used in the χ^2 calculations.

Figure S2. Region 2 relative sea level measurements and predictions. Sea level measurements and curves are plotted as described in the caption to Fig. S1.

Figure S3. Region 3 relative sea level measurements and predictions. Sea level measurements and curves are plotted as described in the caption to Fig. S1.

Figure S4. Region 4 relative sea level measurements and predictions. Sea level measurements and curves are plotted as described in the caption to Fig. S1.

Figure S5. Summary of χ^2 misfit values of ICE-5G (black squares), Laur16 (light grey circles), and ICE-6G (dark grey diamonds) to all RSL measurements in Regions 1–4. Shown are χ^2 misfit values for each of the individual RSL sites, as well as the cumulative χ^2 misfit values for each region ('Reg. 1', 'Reg. 2', 'Reg. 3', and 'Reg. 4') and all regions ('All'). All χ^2 values are calculated using the site-specific cut-off time for the data described in Section S2. RSL site names are defined in Fig. 2 of the main text.

Figure S6. Scaling factors applied to the ICE-5G model to derive the Laur16 model.

Table S1. Goodness of fit (mean squared error in $mm^2\ yr^{-2}$) of GIA model predictions to GPS-derived vertical crustal motion for 18 GPS sites in northern Canada. The GIA models are ICE-5G (Peltier 2004), Laur16 (this study), and ICE-6G (Peltier *et al*. 2015). The mean squared error values are shown for regions R1 + R2, R3 and R4, as well as for the total of regions R1–R4. The mean squared errors are given for GPS-observed vertical crustal motion used in this study (top) and from Peltier *et al*. (2015) (bottom). Elastic correction refers to the elastic response to present-day ice mass change discussed in the main text. The elastic correction is included in the calculation of the mean squared error unless otherwise indicated.

Table S2. Measured absolute horizontal motions[1] for GPS Sites (in millimetres per year).

(http://gji.oxfordjournals.org/lookup/suppl/doi:10.1093/gji/ggw103/-/DC1).